TECHNICAL MEMORANDUM

334

Climatologies of sensitive areas for short term forecast errors over Europe – EUMETNET-EUCOS study

G.J. Marseille and F. Bouttier

Research Department

April 2001

European Centre for Medium-Range Weather Forecasts
Europäisches Zentrum für mittelfristige Wettervorhersage
Centre européen pour les prévisions météorologiques à moyen

Contents

Chapter 1

Introduction

The present document is the final report for the EUMETNET (European Meteorological Network) community to produce climatologies of sensitive areas of 2-day forecast errors over Europe as part of the EUCOS (EUMETNET Composite Observing System) program. The objective of EUCOS is to improve the quality and make more cost-effective the numerical and general forecast at European scale. The basic idea is to consider a reduction of the ground-based radiosonde network on the European continent and to compensate this reduction by a higher observation density in data sparse areas surrounding the territory of EUMETNET members, including the Mediterranean and Baltic seas and the oceans. Climatologies of sensitive areas as produced in this study can be used to develop strategies on where to operate new observation systems in the near future to improve the 2-day forecast over Europe. More detailed information on EUMETNET and EUCOS is found in [1] and the EUMETNET internet pages (http://www.eumetnet.eu.org/).

Short-term forecast errors are mainly due to errors in the forecast initial state. This study aims at identifying those areas over Europe and its surrounding areas where small errors in the initial state can have a relatively large impact on 2-day forecast errors in predefined so-called targeted areas. This requires the definition of a 'diagnostic' function that measures the forecast quality as a function of the forecast initial condition. Partial derivatives of the diagnostic function with respect to the initial condition measure the sensitivity of forecast errors to changes in the initial conditions and are denoted 'sensitivities'. In this study we consider two targeted areas representing Northern and Southern Europe. For both areas, sensitivities are produced for three winter and three summer months. They are archived and averaged as climatologies which will serve as a basis to decide on the positioning of new observation systems in data sparse areas near Europe to improve the 2-day forecast over Europe.

ECMWF produces sensitivity diagnoses for the Northern Hemisphere operationally since 1994. The operational sensitivity suite will serve as a basis for the configuration of the experimental setup for the EUCOS study and is discussed briefly in Chapter 2 together with the necessary modifications to meet the EUCOS requirements, see [1]. The resulting configuration will produce and archive sensitivities for the two targeted areas for the winter and summer periods. The operational sensitivity suite offers a couple of options for sensitivity production. In addition to the EUCOS requirements to produce and archive so-called scaled gradients, we decided to produce and archive so-called 'key analysis errors'. They have some advantageous properties compared to scaled gradients in validating the configuration and interpretation of the sensitivity fields as discussed in section 2.1.

The output of the experiments will be an archive of sensitivity fields, including both scaled gradient fields and key analysis error fields, for the targeted areas for the winter and summer periods. For an impression of the archived sensitivity fields and their ability to correct the 2-day forecast error, some interesting case studies are discussed chapter 3. Next, the archives are integrated in Chapter 4 to produce climatologies of sensitive areas. The results are summarized in chapter 5 together with a discussion on the interpretation and limitations of sensitivity studies for observation planning.

Chapter 2

Sensitivity experiment configuration

This chapter describes briefly the operational sensitivity suite at ECMWF and the necessary modifications to meet the EUCOS requirements, see [1]. The resulting configuration will produce archives of sensitivities and key analysis errors for two targeted areas, representing Northern and Southern Europe, and three winter and three summer months. The next section describes the technical framework of the configuration. The remaining sections discuss technical and methodological details. Section 2.2 discusses the performance of the T63L60 model that is used for the 2-day forecast trajectory. Its performance is verified against the operational higher-resolution T319T60 model. Section 2.3 discusses the use of sharp boundaries in limited area targeted areas that might give rise to spurious effects of vorticity and divergence near the boundaries. The impact of these boundary effects on the sensitivity computations is checked by smoothing the edges of the targeted areas. Finally, the operational sensitivity suite employs a simplified package of physics for the adjoint integrations. In section 2.4 we studied the impact of implementing a more elaborate physics package for the adjoint integrations.

2.1 Technical framework

This section briefly describes the experimental setup of the sensitivity suite currently operational at ECMWF. The basic idea is that short-term forecast errors are mainly due to errors in the forecast initial state rather than model errors. To improve the short-term forecast we need some kind of measure that relates forecast errors to its initial state. Forecast error is defined as the difference between the forecast and a verifying atmospheric state. To limit the computational burden, the forecast initial state is truncated at resolution T63L60 and the forecast is run at T63L60 using non-linear physics, no ozone and no wave coupling. The validity of this approach is discussed in the next section. The operational suite includes several choices for the verifying atmospheric state. We choose the operational analysis at verification time, truncated at T63L60. A diagnostic function (also denoted cost or objective function) J is defined as an energy norm of the forecast error, evaluated at the targeted area, see also [2]:

$$J(x_0) = \frac{1}{2} < M(F(x_0) - x_t), M(F(x_0) - x_t) > \tag{2.1}$$

$<,>$ denoting inner product, x_0 and x_t denote the initial analysis at time t_0 and verifying analysis at $t = t_0 + 48$ respectively, F is the forecast model integrating the intitial state x_0 forward in time and M a mask operator corresponding to the targeted area, see also Fig. 2.1. The energy norm is defined as an integral on the sphere according to [3, 12]:

$$< x, x >= \frac{1}{2}\int_0^1 \int\!\!\int_\Sigma [\nabla\Delta^{-1}\zeta\cdot\nabla\Delta^{-1}\zeta + \nabla\Delta^{-1}D\cdot\nabla\Delta^{-1}D + R_aT_r(\ln p_s)^2 + (C_p/T_r)T^2]\mathrm{d}\Sigma(\frac{\partial p}{\partial\eta})\mathrm{d}\eta \tag{2.2}$$

with x defining the atmospheric state with components ζ, D, p_s and T, *i.e.* vorticity, divergence, surface pressure and temperature respectively, p is pressure, Σ denotes the horizontal integration

domain on the sphere, η is the vertical coordinate, T_r is a reference temperature set at 300 degrees Kelvin and R_a and C_p are thermodynamic constants and denote the gas constant for dry air and dry air specific heat respectively; $R_a = 287JK^{-1}kg^{-1}$, $C_p = 1004JK^{-1}kg^{-1}$. Motivation for the choice of the energy norm as a metric for predictibility problems is discussed in [12].

Eqs. (2.1) and (2.2) relate forecast initial state to forecast errors on the targeted areas. As a first order approximation, a change δx_0 in the initial conditions x_0 results in a change of forecast error J given by $\delta J =< \nabla J_0, \delta x_0 >$, meaning that in regions where the gradient ∇J_0 is large, a change in initial conditions has a large impact on the forecast error. Hence, the pattern of the gradient of J at initial time 0 shows the sensitivity of the forecast error to the initial conditions. As explained in [2] the gradient corresponds to the most rapidly growing components of the analysis error.

Computation of the cost function gradient at initial time requires integration of the adjoint model as explained in e.g. [2], [3], [5]. The adjoint integrations are performed in the vicinity of the trajectory as derived by the forward integration using the T63L60 model. The limitation of the adjoint integrations is that they are linear and can only describe the sensitivity to small initial perturbations for which the time evolution can be described by the tangent linear model. In the EUCOS study we limit the forecast range to 48 hours. The choice of model physics in the tangent linear model is discussed in section 2.4.

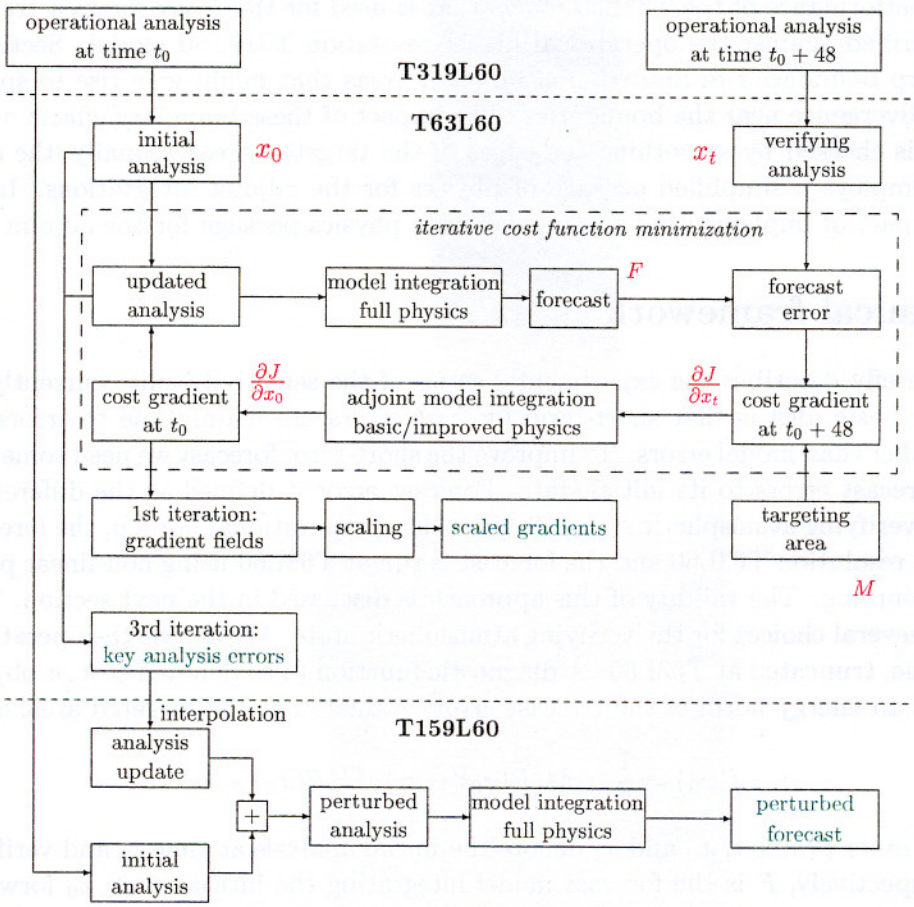

Figure 2.1: ECMWF configuration of technical framework for the production of sensitivities, key analysis errors and perturbed forecasts.

All previously described steps are displayed in Fig. 2.1, which describes schematically the configuration for sensitivity experiments at ECMWF. The scheme describes an iterative procedure to minimize

the cost function J. The cost function gradient, ∇J_0, at the first iteration provides sensitivities after proper scaling.

2.1.1 Gradient scaling

To arrive at the sensitivities, a proper linear scaling has to be applied to the cost function gradient. To determine this scaling factor, we rewrite the diagnostic function in matrix-vector form as $J = (F(x_0) - x_t)^{\mathrm{T}} M^{\mathrm{T}} C M (F(x_0) - x_t)$, with C the positive definite weight matrix containing the weight factors in Eq. (2.2), including the layer depth Δp. We can now write for the cost function gradient to the initial condition:

$$\nabla J_0 = F'^{\mathrm{T}} M^{\mathrm{T}} C M (F(x_0) - x_t) \tag{2.3}$$

with $F' = \nabla F(x_0)$, *i.e.* F linearized at x_0. Eq. (2.3) can be used in an optimization procedure to minimize the cost function J. Gradient methods such as steepest descent or conjugate gradients provide an update of the state linearly in the gradient direction: $\delta x_0 = -\alpha \nabla J_0$. The Gauss-Newton method uses the second derivative of the cost function to get the state update:

$$\begin{aligned} \delta x_0 &= -[\nabla^2 F(x_0)]^{-1} \nabla J_0 \\ &= -[F'^{\mathrm{T}} M^{\mathrm{T}} C M F']^{-1} \nabla J_0 \end{aligned} \tag{2.4}$$

Considering the special case of a linear forecast model F, Eq. (2.3) is an exact quadratic cost function, $F(x_0) = F x_0$ and F' equals F. Substituting in Eq. (2.4) and assuming all matrices are invertible we have $\delta x_0 = -x_0 + F^{-1} x_t$ as expected, *i.e.* one iteration provides the optimal solution for an exact quadratic cost function.

In the ECMWF configuration however F is a non-linear model at resolution T63L60 and F'^{T} is the adjoint of the tangent linear model used in the adjoint integrations. The matrix of second derivatives of cost function J is positive definite and may thus be written as $S \Lambda S^{-1}$ with Λ a diagonal matrix of positive eigenvalues of $\nabla^2 F(x_0)$ and S an orthonormal matrix build up of its eigenvectors. As explained in [2] the sensitivity pattern is dominated by the eigenvectors with the largest eigenvalues. The scaling factor should therefore be proportional to the inverse of the largest eigenvalue of the matrix $\nabla^2 F(x_0)$. In practice a less advanced scaling procedure has been implemented by considering the energy norm (matrix C) only. This simplified processing imposes a drawback on the interpretation of the sensitivity fields and this is one of the reasons to consider key analysis errors in addition.

2.1.2 Key analysis errors

In addition to the contract requirements we will configure the experimental setup to compute key analysis errors besides the sensitivity fields. This facility is already available in the operational suite. There are a couple of reasons for this additional effort

- As said in the previous section, scaling of the cost function gradient to derive sensitivity fields is not a trivial step. The current implementation is not optimal, making the meteorological interpretation of the sensitivity fields difficult.
- Key analysis errors are obtained from minimizing the diagnostic function in 3 iterations, see Fig. 2.1. The scaling of gradient fields is not an issue in this case, as it is part of the optimization procedure. More than 3 iterations does not provide a better estimate of the analysis errors, mainly because of the discrepancy between the forecast model F and adjoint model F', see [6].
- In [6] it was concluded that key analysis errors represent an improved estimate of analysis errors compared to the scaled gradient. It was found that the scaled gradient projects mainly on the fastest growing forecast errors. The closer correspondence of evolved key analysis errors and forecast errors show that key analysis errors are more realistically projecting on to the full analysis errors.

- The operational suite at ECMWF permits subtracting the key analysis errors from the operational analysis interpolated at T159L60 and by running a 10-day forecast with a T159L60 model with full physics, see Fig. 2.1. The resulting so-called sensitivity or perturbed forecasts may be verified against perturbed forecasts from the operational suite to check the reliability of the experimental configuration, see section 2.5. Moreover, this provides a good measure of the performance of the T63L60 adjoint model in explaining initial errors.

Based on the considerations above we decided to archive the key analysis errors in addition to the scaled gradients. Chapter 4 discusses the main differences between both sensitivity fields and it is motivated which fields to use in the production of the climatologies. It is at least scientifically interesting to compare climatologies from both approaches.

2.2 T63L60 forecast performance

The 48-hour forward integration of the initial analysis is performed with the operational ECMWF model at resolution T63L60 using full physics, no ozone and no wave coupling. This provides the trajectories needed for the adjoint integrations. To properly investigate the sensitivity of the 48-hour forecast errors to the forecast initial conditions, the performance of this model should be close to the performance of the operational higher-resolution T319L60 forecast model for the targeted areas and forecast periods of interest.

To check the performance of the T63L60 model, one month of forecasts have been produced with the T63L60 model and verified against forecasts from the operational T319L60 model. The average scores indicate that the performance of the T63L60 model is very acceptable with 97% anomaly correlation of the 500 hPa forecast over Europe at the for EUCOS interesting 48-hour range, *i.e.* only 1% lower than the T319L60 model, see Fig. 2.2. The scatter plot in Fig. 2.3 shows that the T63L60 model performs sometimes even better than the T319L60 model over Europe. From these results we conclude that the T63L60 model is decent enough in the short range over Europe to serve as linearization trajectory for the adjoint integrations.

2.3 Targeted area boundaries

The diagnostic function defined by Eq. (2.1) provides a measure of forecast errors evaluated at the targeted area through the mask operator M. The targeted area in the operational ECMWF sensitivity suite is the extratropical Northern Hemisphere (30^0-90^0N). For the EUCOS study we changed the geographical domains of the targeted areas according to the study requirements [1] to: (see Fig. 2.4)

- Northern Europe : 10W - 35E, 45N - 65N
- Southern Europe : 10W - 35E, 30N - 50N

We considered the use of sharp boundaries that might give rise to spurious vorticity and divergence effects near the boundaries. In the IFS, the mask is applied to horizontal wind components, temperature and surface pressure. However, the forecast error diagnostic function is defined by a global norm of vorticity, divergence, temperature and surface pressure, see Eq. (2.2). Wind truncation on the mask edges leads to high values of vorticity and divergence, which contribute spuriously to the forecast error norm and resulting sensitivities. A possible solution of this problem is to smooth the edges near the boundaries. This has been investigated for the Northern Europe domain on a single case. Sensitivities, key analysis errors and score plots have been produced for the forecast error at 28 December 1999 both for a rectangular mask with sharp boudaries and a mask that smoothes the edges linearly over 10 degrees in both latitude and longitude. The corresponding sensitivities showed no significant differences [7], meaning that spurious vorticities and divergencies at the area boundary

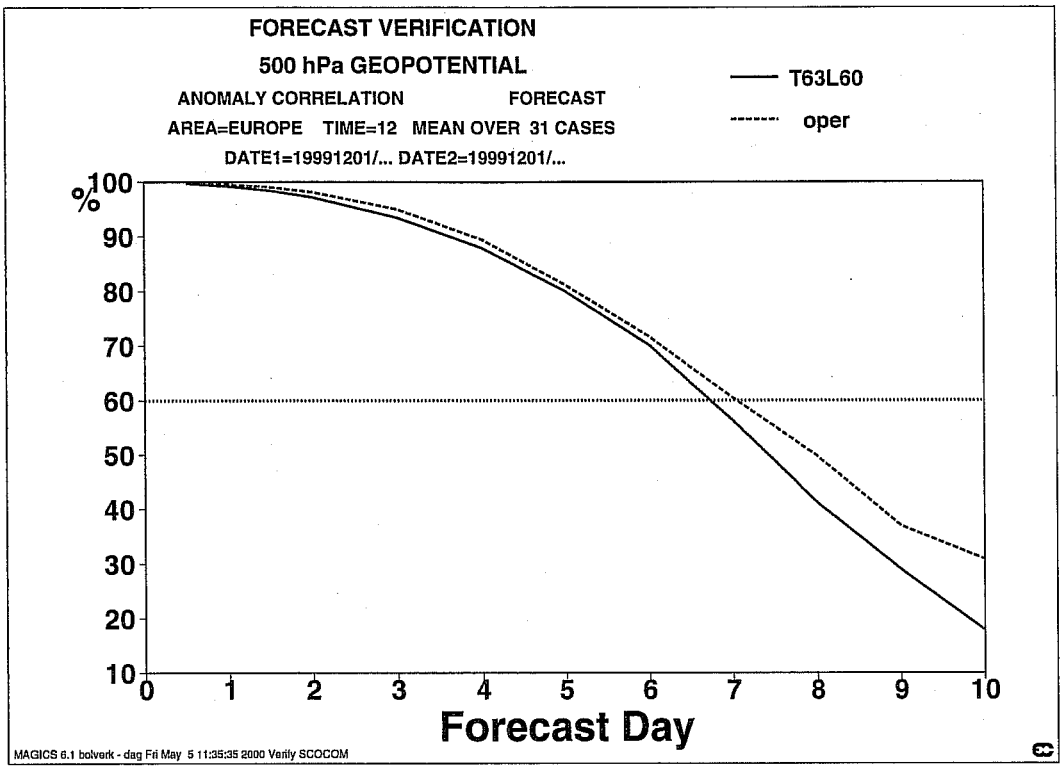

Figure 2.2: T63L60 forecast model performance (solid) line) verified against the operational higher-resolution T319L60 model (dashed line) for December 1999. One month average of geopotential height anomaly correlation over Europe at 500hPa.

are negligable and have little impact om the forecast error, probably because the EUCOS domain is large enough. The key analysis errors were subtracted from the initial analysis to obtain the so-called perturbed analysis. Next, a perturbed forecast was procduced using a full physics non-linear model at resolution T159L60, see Fig. 2.1. This procedure was performed for the key analysis errors produced with and without the smoothing procedure described above. The quality of the perturbed forecasts are compared in Fig. 2.5. The score plot shows no significant differences in the first couple of days, as expected from the very small impact on sensitivities by smoothing the edges. The large deviation after six days is mainly caused by a small difference of the jet stream position that enters the scores area North of England at forecast day 6. This difference evolves in time, moving eastwards and growing in strength. Its position remains in the scores area up to day ten, which explains the deviation of both scores.

2.4 Physics packages

The operational suite at ECMWF currently performs the adjoint integration using a tangent linear model with basic physics, *i.e.* simplified parameterizations of surface drag and vertical diffusion, [8]. Recently, improved linearized physical parameterizations have been developed at ECMWF for the tangent linear and adjoint versions of the ECMWF global forecast model. The physical processes included are vertical diffusion, subgrid-scale orographic effects, large scale condensation, long-wave radiation and deep cumulus convection. A detailed description is provided in [9], which shows that the inclusion of a tangent linear model, including these physical processes fits better to the non-linear model compared to an adiabatic (simplified) version of the tangent linear model. It appears that the

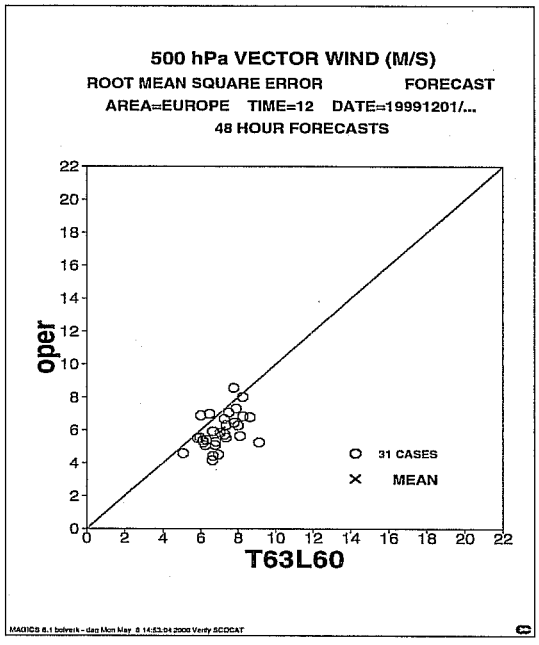

Figure 2.3: Same as Fig. 2.2. The scatter plot shows the distribution of 2-day forecast errors for the wind vector over Europe at 500hPa for 31 days.

adiabatic model mainly resolves large-scale structures of the atmospheric flow while the inclusion of the linearized physics package resolves smaller scale physical processes. In the sequel we shall refer to these two linearized physics packages as i) the 'basic' package for the simpler one as documented in [8] and ii) the 'improved' package for the better one as documented in [9].

The improved physics package has been implemented in the operational 4D-Var data assimilation system at ECMWF. It was shown that its inclusion significantly improves the behaviour of the tangent linear model with respect to the non-linear model, [10]. Based on these promising results we decided to extend the operational sensitivity suite by adding the possibility to include the improved physics package. The increase of computational cost is about 50% compared to the basic physics package.

Fig. 2.6 displays the sensitivities of 2-day forecast errors to initial conditions for adjoint computations performed with and without inclusion of the improved physics package. They show correcting structures of the wind vector (arrows) and surface pressure fields (colours) at model level 60 to be applied to the forecast initial state at 26 December 1999 12UTC in order to reduce the 2-day forecast error. Both figures shows similar structures, but more intense for the simplified physics package. Further discussion on the impact of the choice of linear physics package on sensitivities is postponed until the next chapter when discussing climatologies of sensitive areas.

2.5 Configuration validation

The technical framework for the EUCOS experiments has been validated by comparing 3-month average scores of perturbed forecasts of the experimental setup against those from the operational suite. Remember that the operational sensitivity suite aims at minimizing the 2-day forecast error on the extratropical Northern Hemisphere, while the experimental setup for EUCOS aims at the Northern Europe domain. For this purpose, a special configuration of the forecast verification package has been developed in order to produce score computations on the EUCOS domains.

Figs. 2.7a and Figs. 2.8a display scores of perturbed forecasts up to 3 days for the operational suite and the configuration for the EUCOS Northern Europe target area. They show that the operational suite performs better on the extratropical Northern Hemisphere which is not surprising since the

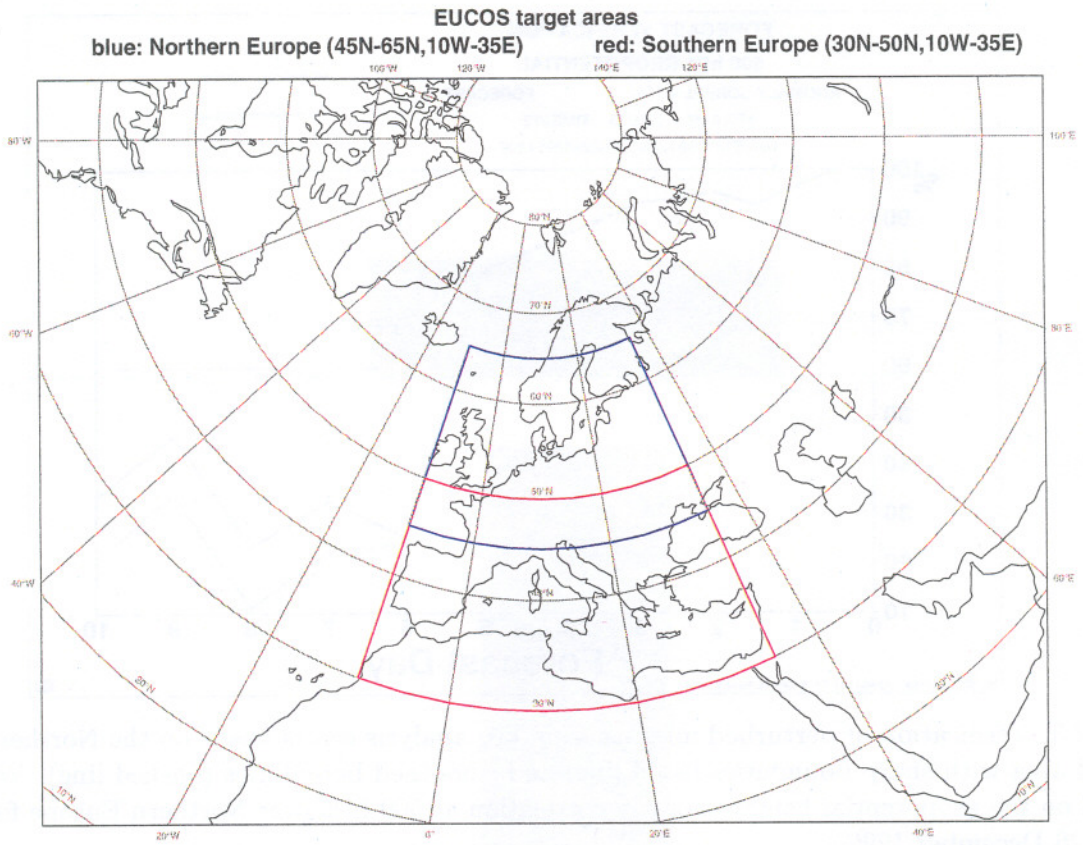

Figure 2.4: EUCOS target areas. The blue area represents Northern Europe, the red area Southern Europe.

targeted area of the operational suite is in fact the extratropical Northern Hemisphere. On the other hand, for the the Northern Europe area Figs. 2.7b and Figs. 2.8b show a better performance of the experimental setup in the first 2 to 3 days. The inclusion of the more elaborated linear physics package has no significant impact on the forecast scores on average. In the next chapter however, we will show that climatologies derived from both packages may differ significantly. Similar results apply for the Southern Europe target area (not shown here).

Perturbed forecasts beyond three days up to ten days show a better performance of the operational sensitivity suite for all regions in the Northern Hemisphere, due to the limited target areas in the chosen configuration. This proves that the chosen configuration is not a suitable tool to diagnose errors in medium-range weather forecasts. It is only supposed to highlight areas where the 48-hour forecast error over Europe is sensitive to errors in the initial analysis.

Also from the scatter plots in Fig. 2.9 it is clear that the operational suite performs better at the Northern Hemisphere, while the experimental setup performs slightly better on the EUCOS target area domain. These results gave us good confidence in the setup of the technical framework. The positive impact of the perturbed forecasts on the forecast scores over Northern Europe also shows that the T63L60 adjoint tangent linear model performs sufficiently well in the adjoint integration.

2.6 Summary

To summarize this chapter, the configuration of the technical framework will produce sensitivities of 2-day forecast errors to initial conditions. Two targeted areas are considered representing Northern

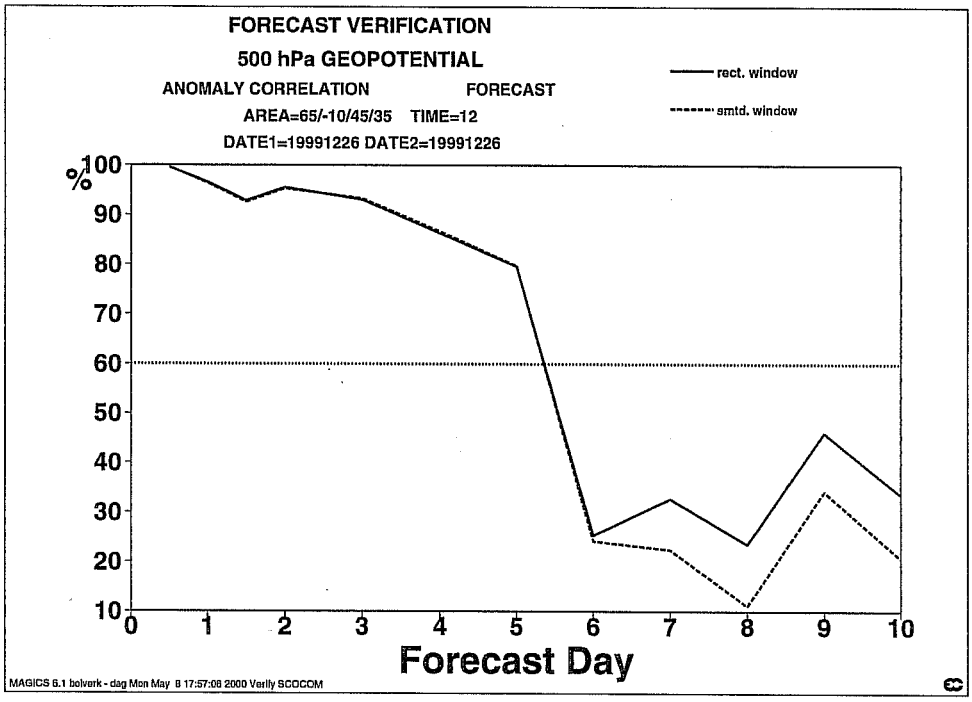

Figure 2.5: Verification of perturbed forecast from key analysis errors based on the Northern Europe targeted area with sharp boundaries (solid line) and smoothed boundaries (dashed line). Verification is based on the geopotential height anomaly correlation at 500 hPa over Northern Europe for a single case at 26 December 1999.

and Southern Europe. Sharp boundaries of the targeted areas appeared to have no detrimental effect on the produced sensitivities. Two 3-months periods are considered representing winter and summer. For both periods and targeted areas, the configuration will produce scaled gradients and key analysis errors. The computations are based on both the basic linear physics package, that is currently operational in the ECMWF sensitivity suite and the improved physics package. Although the choice of physics package has only a small impact on the scores, we decided to use the improved physics in the hope that it provides more physically correct patterns.

It should be noted that the experimental configuration has been chosen to produce sensitive areas for errors in the 48-hour forecast over Europe, *i.e.* areas where the 48-hour forecast error over Europe is sensitive to errors in the initial analysis. Due to the limited target areas it is not a suitable diagnostic tool for errors in medium-range weather forecasts.

a)

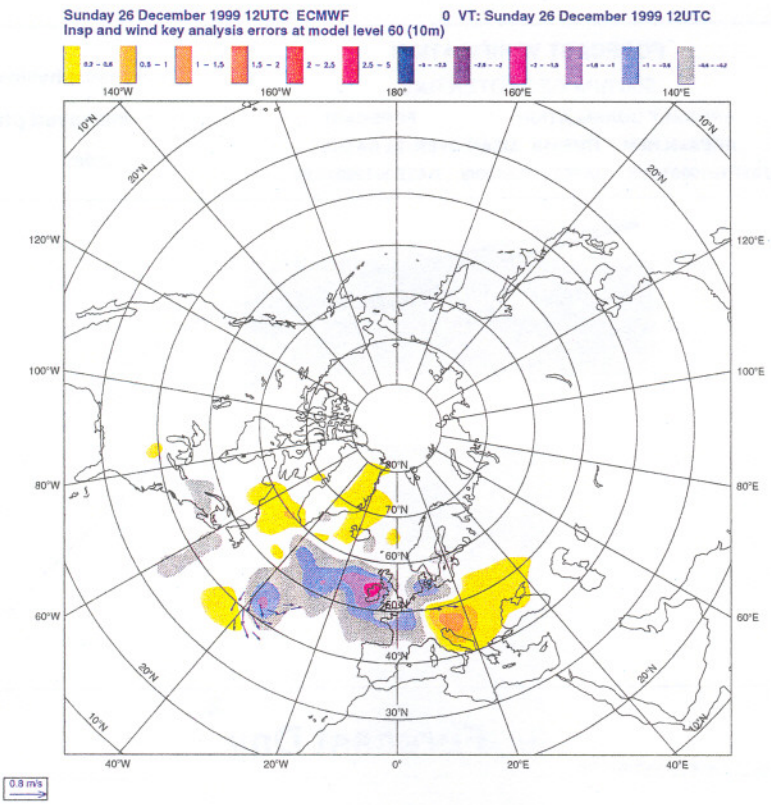

b)

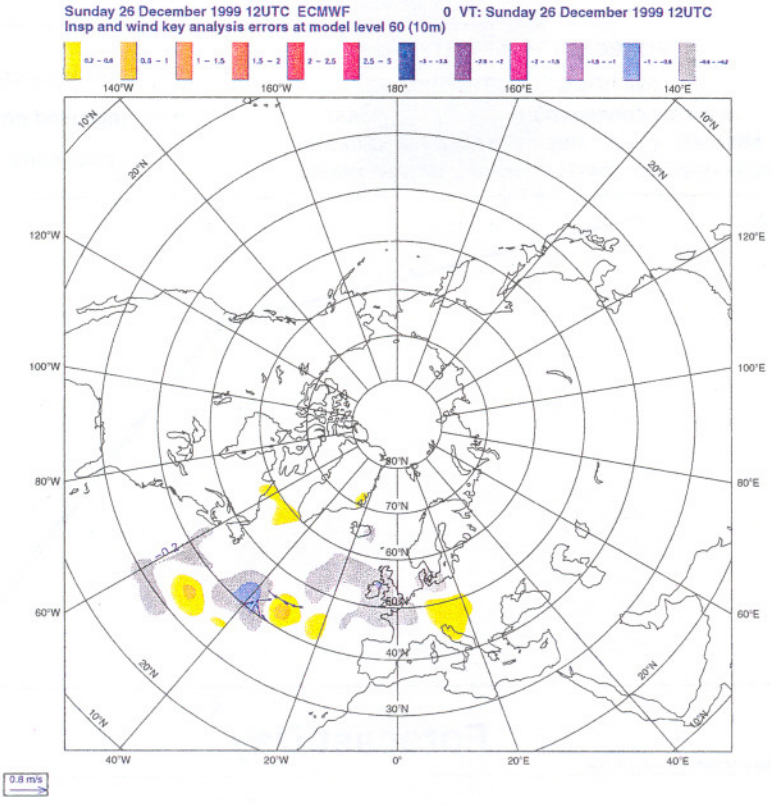

Figure 2.6: Physics package impact in adjoint computations. The figures show sensitivity of forecast errors on 28 December 1999 to initial conditions of wind vector (arrows) and surface pressure (colours) 2 days earlier at model level 60 (*i.e.* 10 m.). The targeted area is Northern Europe. Sensitivities are based on a) the basic and b) the improved physics package. Both figures have identical colours scales.

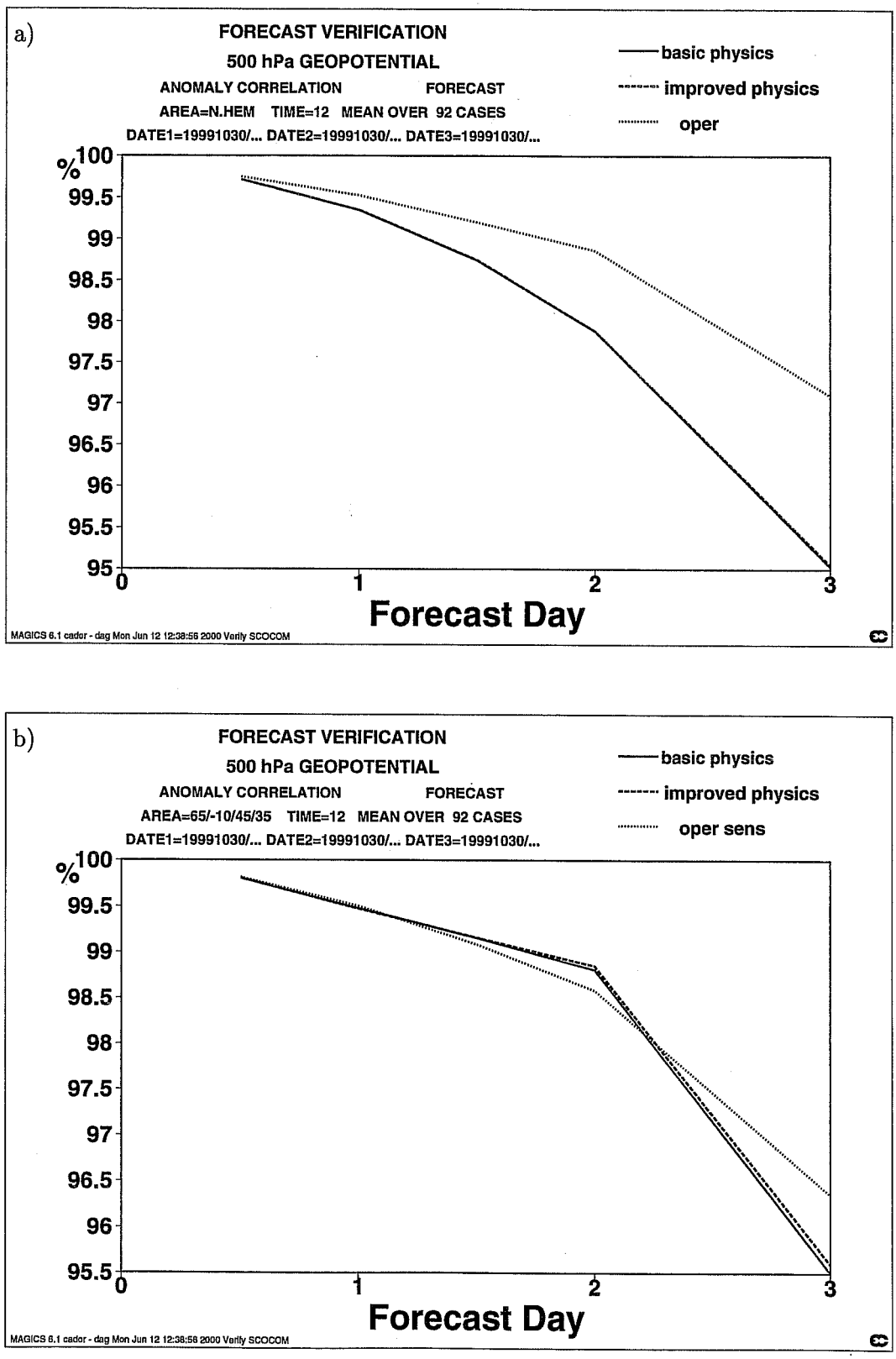

Figure 2.7: Verification of experimental setup with basic physics (red solid line) and improved physics (blue dashed line) against the perturbed forecasts from the operational suite (green dotted line). One month average of geopotential height anomaly correlation at 500hPa for a) the extratropical Northern Hemisphere and b) the Northern Europe EUCOS area.

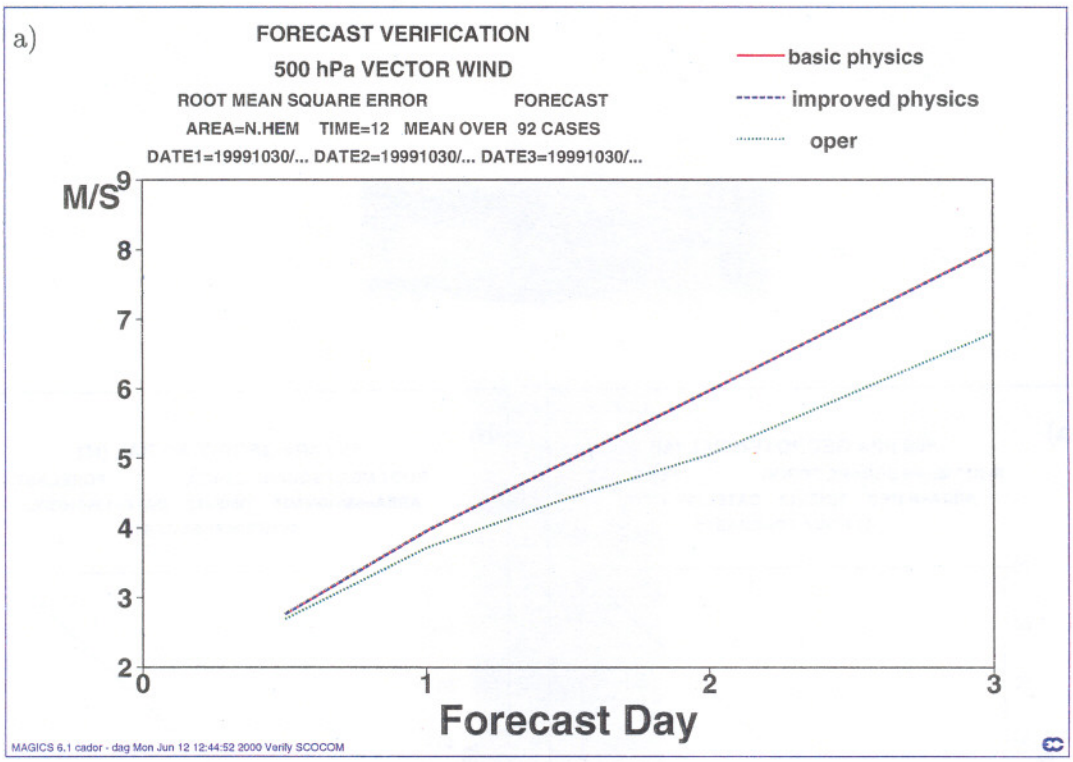

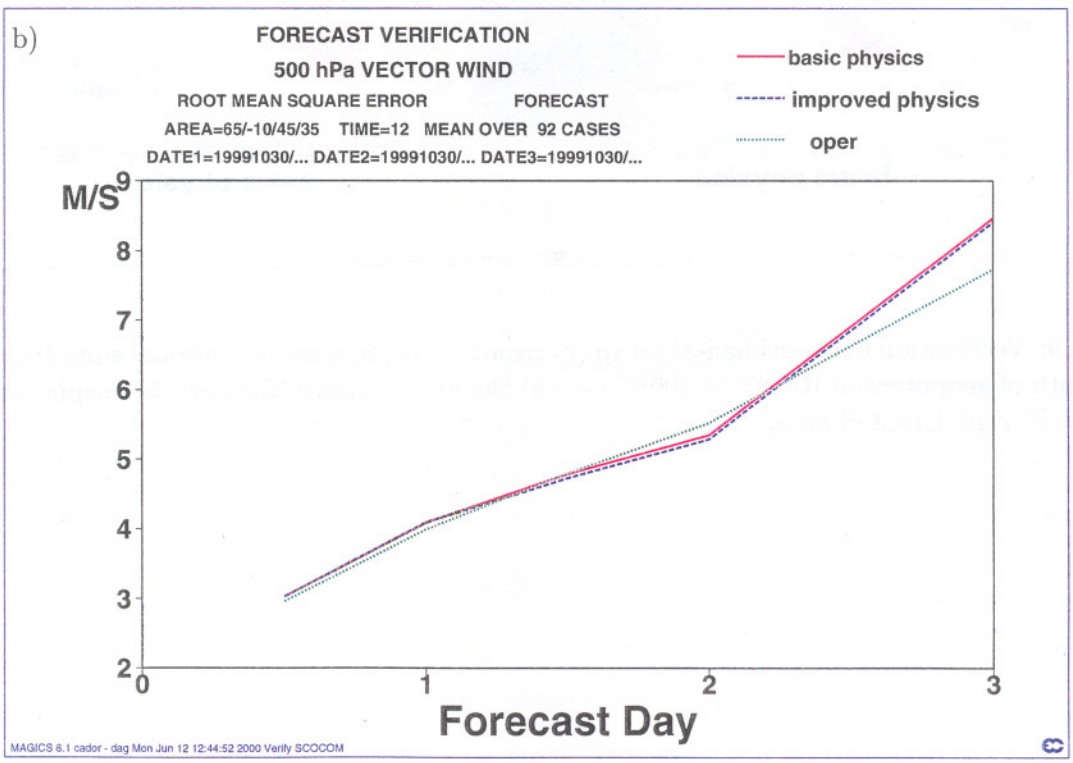

Figure 2.8: Same as in Fig 2.7 but now for one month average of wind vector RMSE at 500hPa.

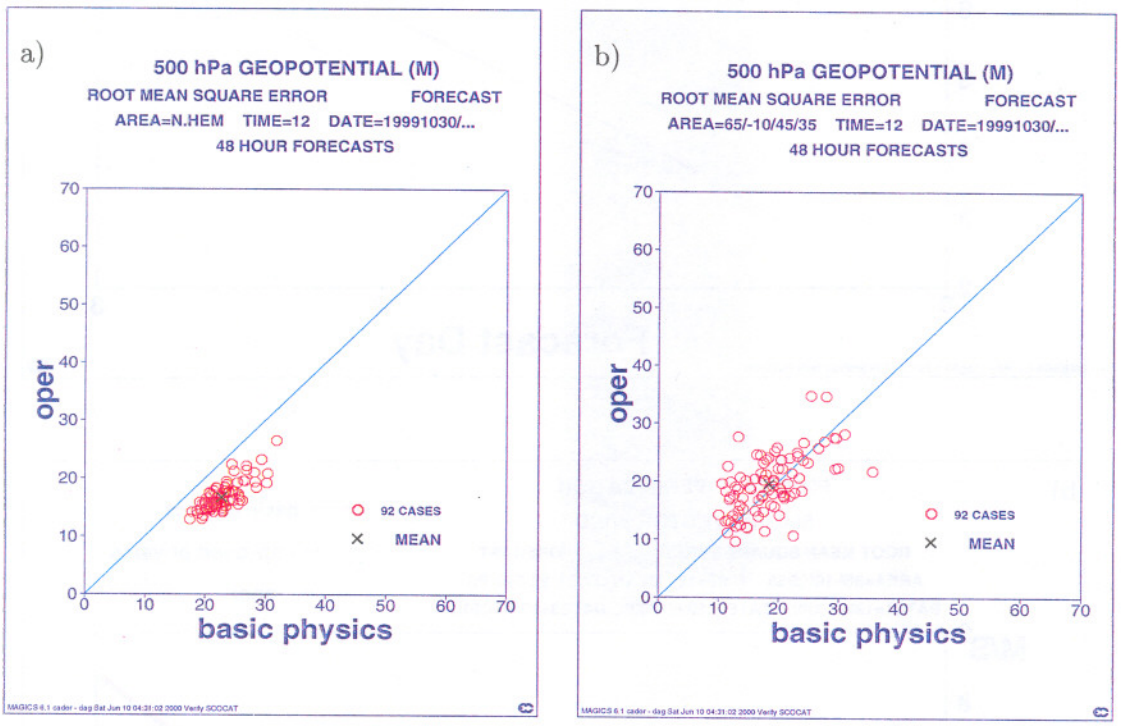

Figure 2.9: Verification of experimental setup (horizontal axis) against operational suite (vertical axis). One month of geopotential RMSE at 500hPa for a) the extratropical Northern Hemisphere and b) the Northern Europe EUCOS area.

Chapter 3

Case studies

This chapter discusses two case studies for which the 48-hour forecast error was larger than average.

3.1 27 December 1999

This case is known as the second Christmas 1999 storm. It is characterized by a fast developping depression between 6 and 12 UTC on 27 December. The depression moves from the South-West of Ireland 20W,48N to the French coast, West of Bretagne 8W,48N and deepens from 993 hPa at 6 UTC to 982 hPa at 12 UTC (ECMWF T319 analyses), see Fig. 3.1a. The depression reaches Bretagne on 17 UTC and reaches its lowest value of 967 hPa on 18UTC at 0W,48N. The 2-day ECMWF forecast of 25 december 12 UTC misses the depression completely, see Fig. 3.1b. The large forecast error is also clear

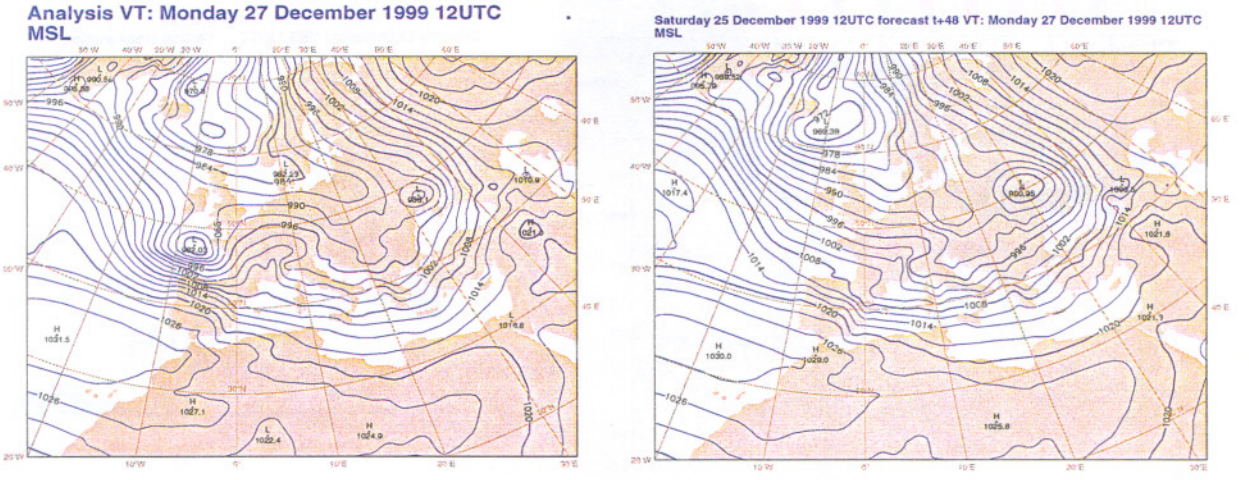

a) b)

Figure 3.1: a) ECMWF operational analysis of mean sea level pressure on 27-12-1999 12 UTC. The minimum pressure value at 8W-48N is 982 hPa. b) Operational 48-hour forecast of 25-12-1999 12 UTC verified on 27-12-1999 12 UTC. The contour interval is 3 Pa.

from Fig. 3.2a, which shows the difference between the operational forecast and analysis. The error in the center of the depression at 8W,48N is 22 Pa. The most sensitive areas of the 2-day forecast error for the Southern Europe target area are located in the Northern Atlantic near the North American coast at 700 hPa, see Fig. 3.3. The 2-day evolution of key analysis errors provides a correction for the operational forecast, see Fig 3.4. Fig. 3.4a shows that key analysis errors do not evolve to the EUCOS target area only. Corrections outside the target area should not be considered as useful corrections to the operational forecast, since forecast errors in these regions are not considered in the

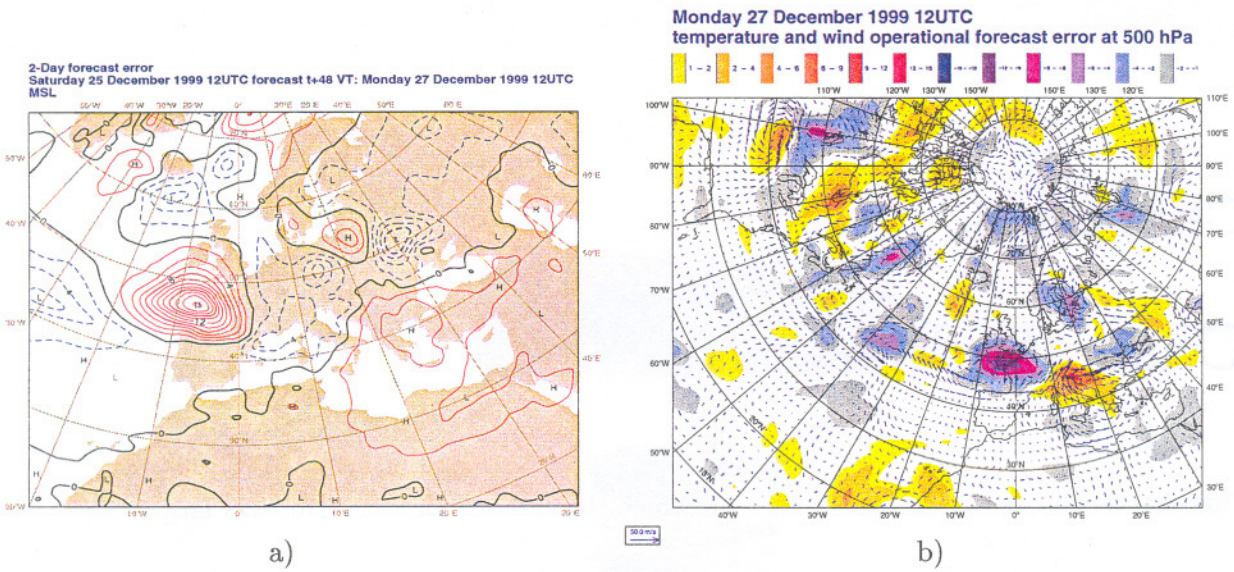

a) b)

Figure 3.2: Operational 2-day forecast error of 25 december 1999 12 UTC verified at 27 december 1999 12 UTC a) for mean sea level level pressure, dashed lines indicate negative values, the contour interval is 2 Pa and b) for temperature (colours) and wind (arrows) at 500 hPa. The wind vector unit length is 50 m/s. Positive/negative colour values (yellow-to-red)/(grey-to-blue) denote an over/under estimate of the forecast temperature.

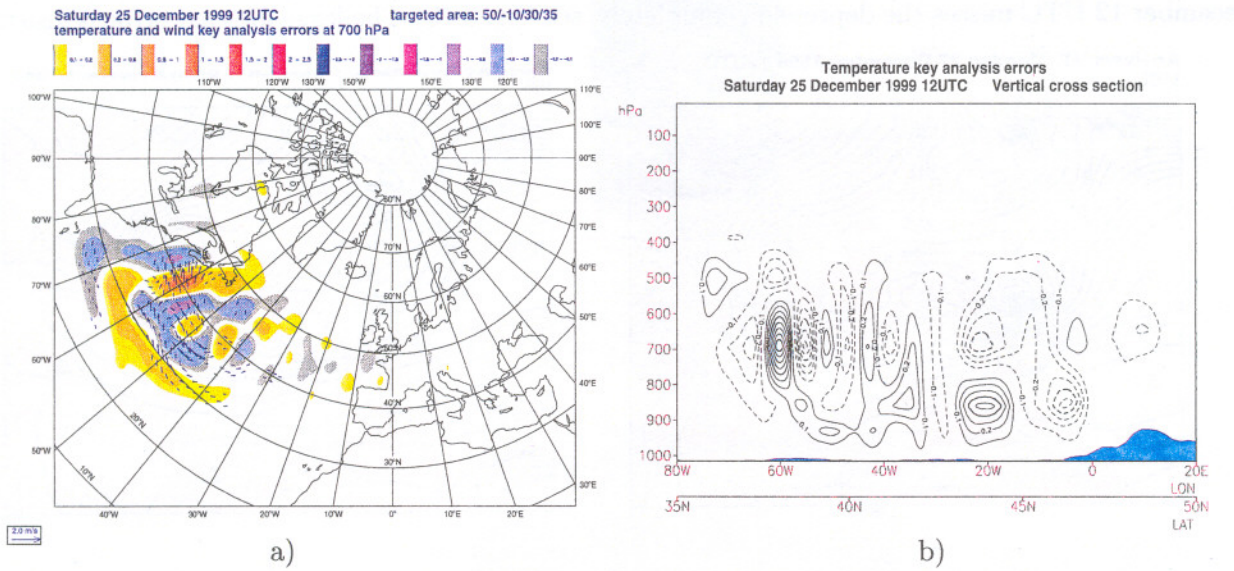

a) b)

Figure 3.3: a) Key analysis errors of temperature and wind at 700 hPa, for 25 december 1999 12 UTC. The target area is Southern Europe. The wind vector unit length is 2 m/s. b) Vertical cross section of temperature key analysis errors across the line from 35N,80W to 50N,20E. Dashed lines indicate negative values. The contour interval is 0.1 degree Kelvin.

diagnostic function. This is also clear by comparing the correction with the forecast error in Fig. 3.2b and shows the limited applicability of the derived sensitivites for short-range forecast error corrections only. Another interesting aspect is the amplitude of the evolved key analysis errors. Although key analysis errors are relatively small, their amplitude increases by a factor of 8 for temperature and up to 25 for the wind vector after 2 days, see Figs. 3.3a and 3.4b. Comparing the mean sea level pressure

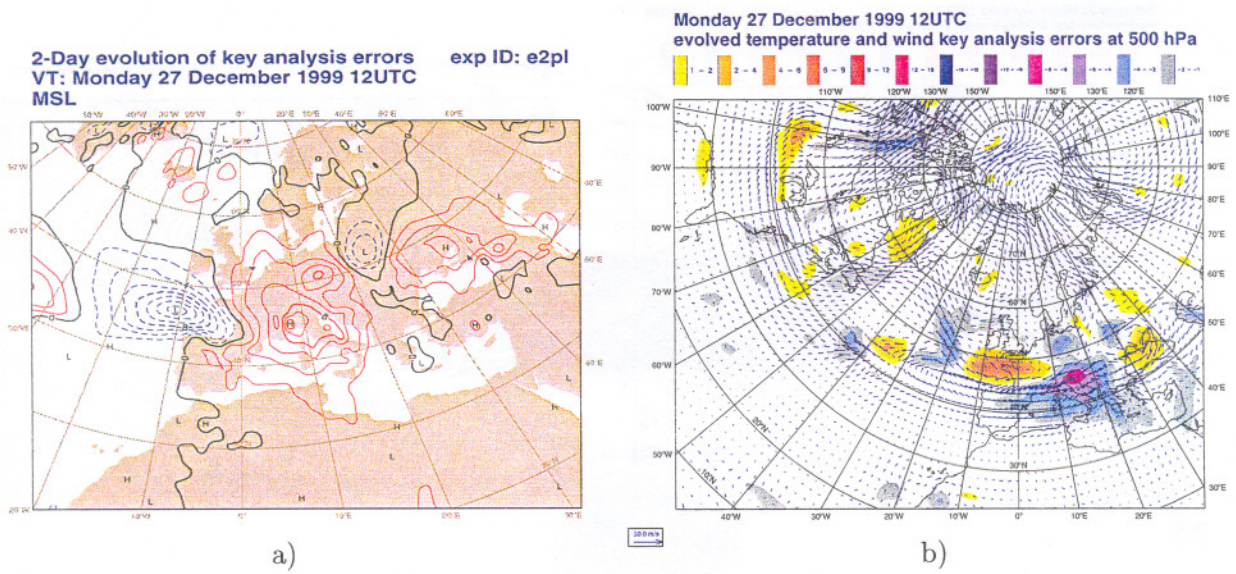

a) b)

Figure 3.4: Impact of 2-day evolution of key analysis errors on a) mean sea level pressure. Dashed lines indicate negative values. The contour interval is 2 Pa. and b) on temperature and wind at 500 hPa. Note the different colour contour intervals compared to Fig. 3.3a which differs roughly by a factor of 8.

correction in Fig. 3.4a with the operational forecast error in Fig. 3.2a, we see that the correction is slightly out of position and the amplitude is too small to correct the forecast error completely. The resulting perturbed forecast is displayed in Fig. 3.5a and shows a significant improvement of

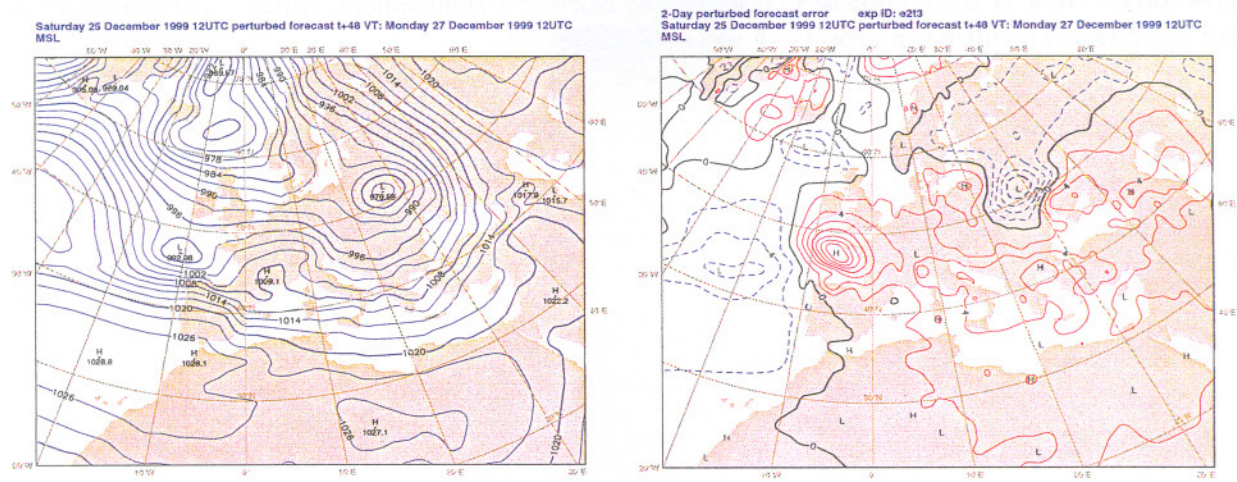

a) b)

Figure 3.5: a) Mean sea level pressure perturbed forecast. The contour interval is 3 Pa. The minimum pressure level value at 11W-47N is 993 hPa. b) Perturbed forecast error of 25-12-1999 12 UTC verified on 27-12-1999 12 UTC. The contour interval is 3 Pa. The error at 11W-47N is about 15 hPa.

forecasting the depression near the French coast. Comparing with the verifying analysis of Fig. 3.1a however shows that the depression is not deep enough and the center is slightly out of position. This is also clear from the perturbed forecast error in Fig. 3.5b. One of the reasons that the key analysis errors correct the operational forecast error only partly is that, unfortunately, the forecast error near the French coast in Fig. 3.2a is not completely captured by the Southern Europe target area. The

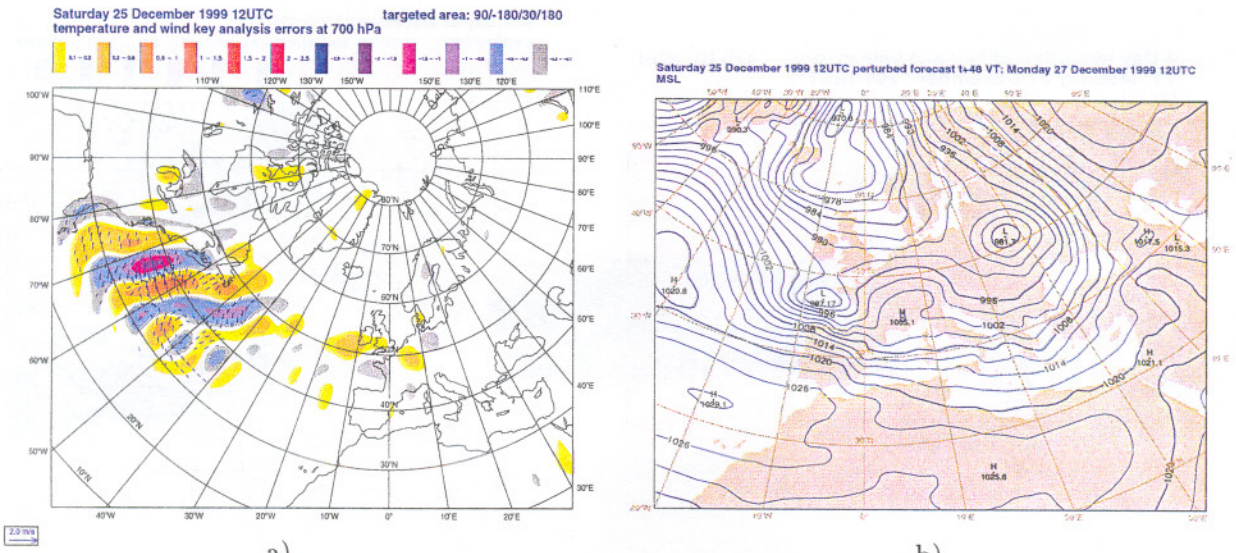

a) b)

Figure 3.6: a) Operational sensitivity suite key analysis errors of temperature and wind at 700 hPa, for 25 december 1999 12 UTC. The target area is the extra-tropical Northern Hemisphere from 30N-90N. b) Corresponding perturbed forecast. The contour interval is 3 Pa. The minimum pressure level value at 8W-47N is 987 hPa.

same is true for the Northern Europe target area. As a result, the key analysis errors from both target areas do not completely capture the error in the initial conditions that resulted in the forecast error near Bretagne. For this case the key analysis errors produced by the operational sensitivity suite, whose target area is the complete extra-tropical Northern Hemisphere, capture the complete initial error conditions, resulting in a better forecast, see Fig. 3.6.

3.2 3 June 1999

This case is characterized by a trough located in the Channel at 500 hPa on 3 June 1999 12 UTC that was not very well covered by the 2-day forecast of 1 June 12 UTC, see Fig. 3.7. The forecast

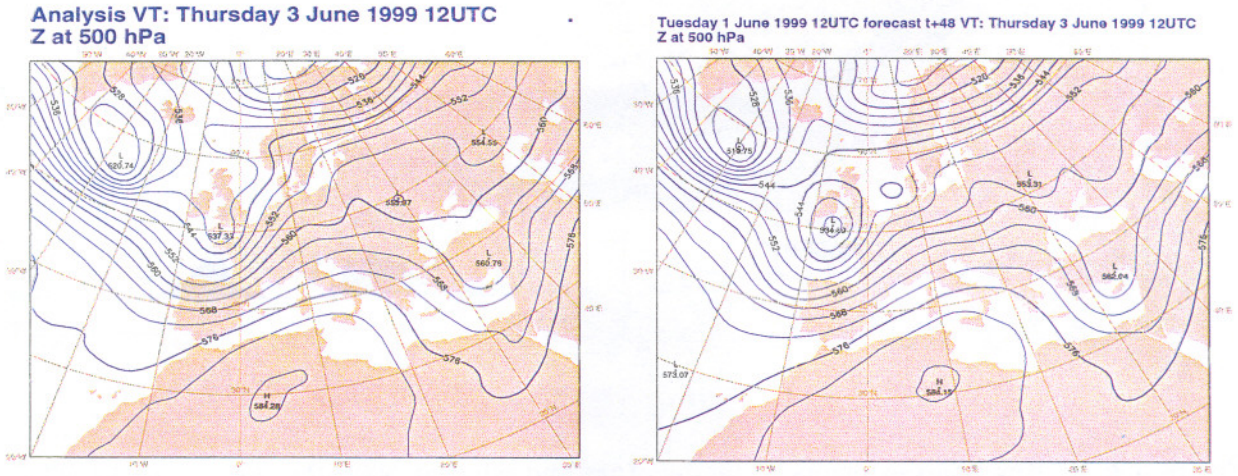

a) b)

Figure 3.7: a) ECMWF operational analysis of geopotential height at 500 hPa on 3-6-1999 12 UTC. A trough is located in the Channel at 4W,50N with minimum pressure of 537 hPa. b) Operational 48-hour forecast of 1-6-1999 12 UTC verified on 3-6-1999 12 UTC. The low pressure field is located at 6W,50N with value 534 hPa. The contour interval is 4 Pa.

error is also clear from Fig. 3.8a, which shows the difference between the operational forecast and analysis. Sensitive areas of the 2-day forecast error for the Northern Europe target area are located

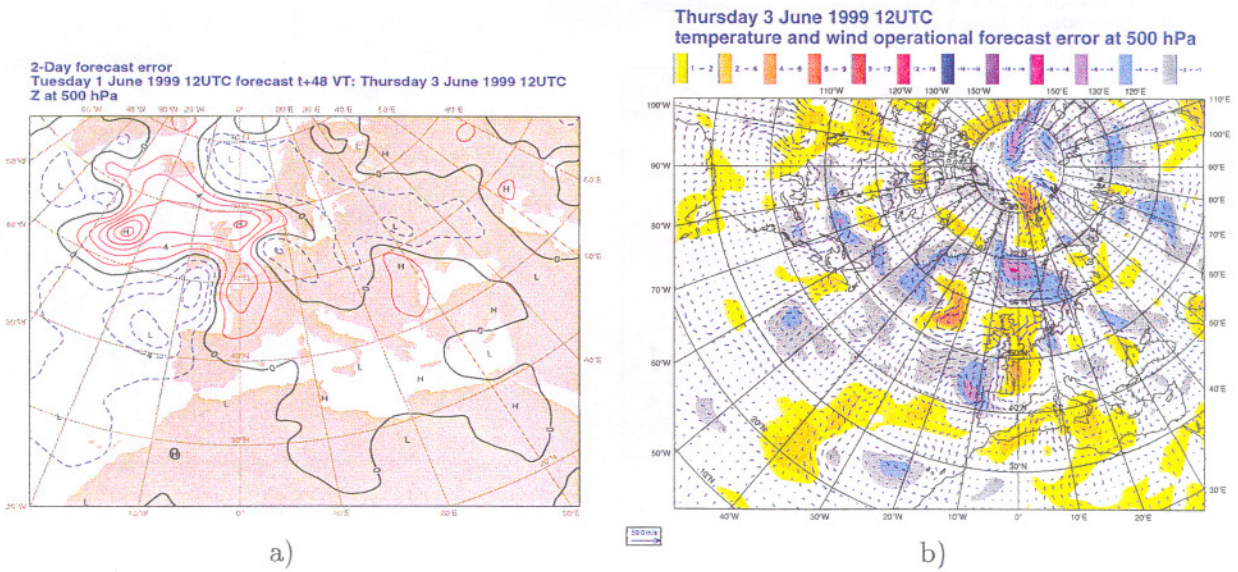

a) b)

Figure 3.8: Operational 2-day forecast error of 1 June 12 UTC verified at 3 June 12 UTC for a) 500 hPa geopotential height. Dashed lines indicate negative values. The contour interval is 2 Pa and b) for temperature and wind at 500 hPa. The wind vector unit length is 50 m/s.

i) over North Africa, the coasts of Spain and France and extend to the coast of Great Britain and ii) the North Atlantic up to the North American coast, see Fig. 3.9. The 2-day evolution of key analysis

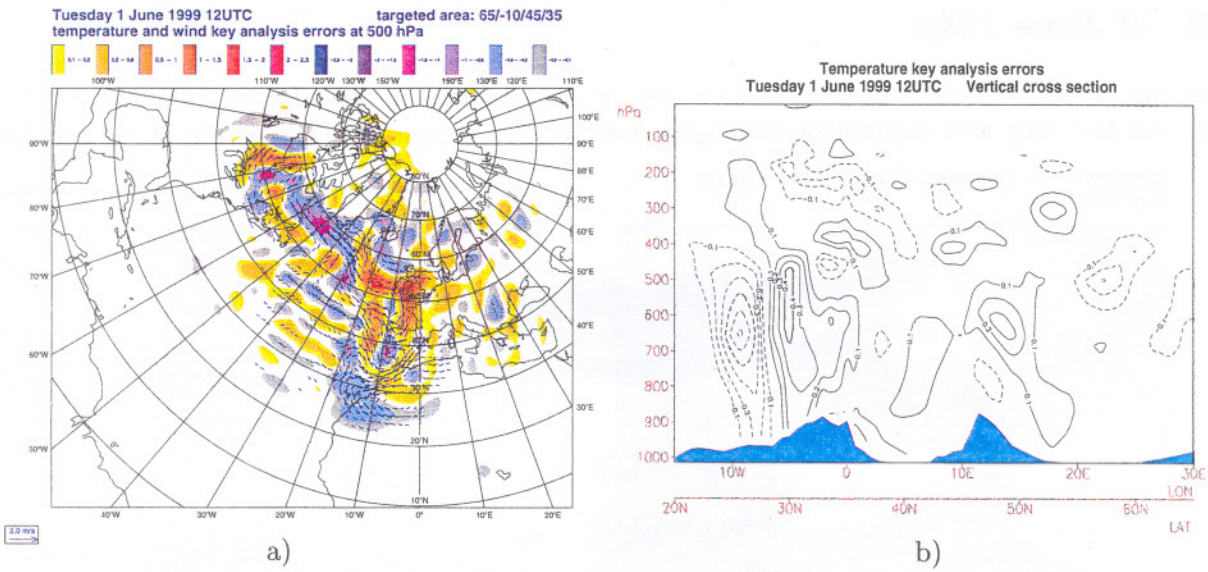

a) b)

Figure 3.9: a) Key analysis errors of temperature and wind at 500 hPa, for 1 June 12 UTC. The target area is Northern Europe. The wind vector unit length is 2 m/s. b) Vertical cross section of temperature key analysis errors across the line from 20N,15W to 65N,30E. Dashed lines indicate negative values. The contour interval is 0.1 degree Kelvin.

errors provides a correction for the operational forecast, see Fig 3.10. As in the Christmas case, the amplitude of the key analysis errors evolves rapidly in time up to factor of 8 for temperature and up to 20 for the wind vector after 2 days. Comparing the 500 hPa geopotential height correction in

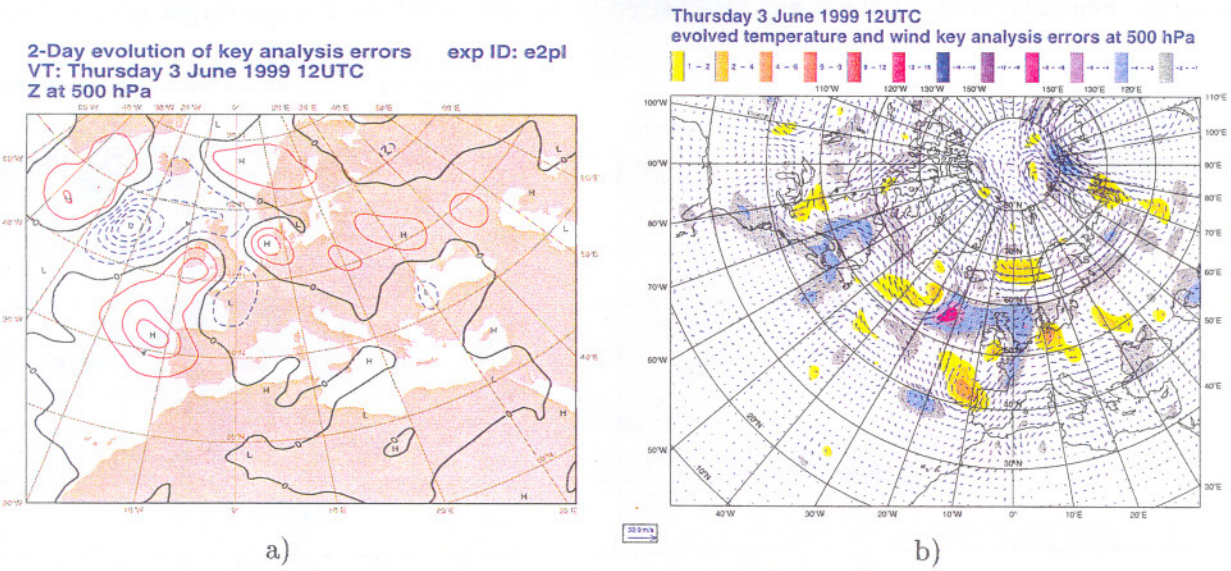

a) b)

Figure 3.10: a) 2-Day evolution of key analysis errors. a) 500 hPa geopotential height. Dashed lines indicate negative values. The contour interval is 2 Pa. b) Temperature and wind. Note the different colour contour intervals compared to Fig. 3.9 which differs roughly by a factor of 3.

Fig. 3.10b with the operational forecast error in Fig. 3.8a, we see, surprisingly, that the correction is very well for the forecast errors at 14W,42N and 23W,55N which are both outside the target area, while the correction for the location of the trough is slightly out of position. As in the previous case,

not all of the interesting forecast error is captured by the target area which might explain the slight misfit. Nevertheless, part of the forecast error has been corrected, in particular at 14W,42N and

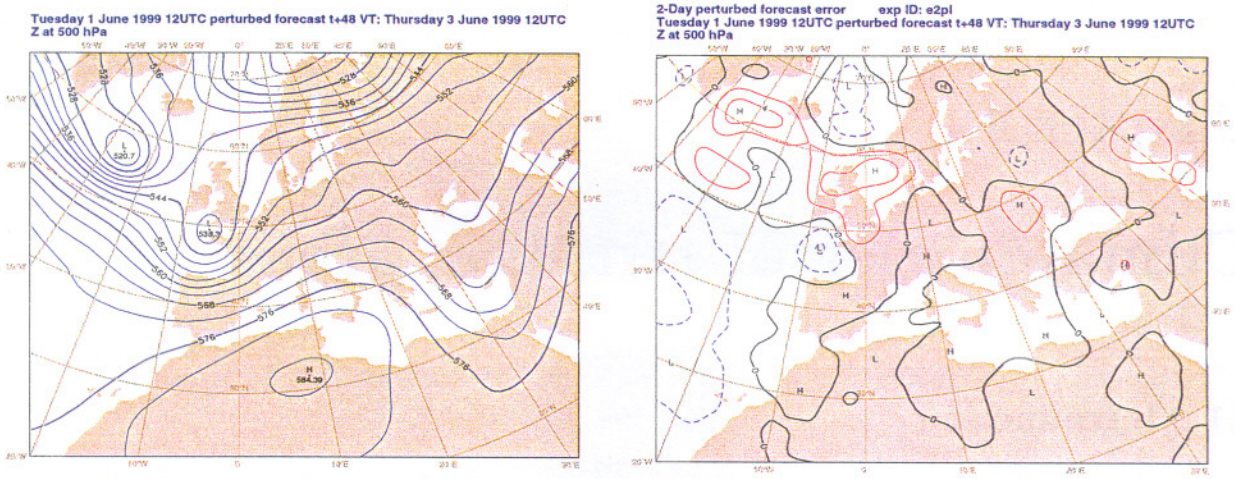

a) b)

Figure 3.11: a) 500 hPa geopotential height perturbed forecast. The contour interval is 4 Pa. The minimum pressure level value at 5W-49N is 538 hPa. b) Perturbed forecast error of 1-6-1999 12 UTC verified on 3-6-1999 12 UTC. The contour interval is 2 Pa.

23W,55N and the small errors over the European continent as displayed by the perturbed forecast and perturbed forecast error in Fig. 3.11.

Chapter 4

Climatologies of sensitive areas

4.1 Introduction

The previous chapter discussed the experimental configuration for the production of sensitivities for the EUCOS interesting European target areas. The production of sensitivities for 2-day forecast errors over Europe included four experiments, that is two target areas (Northern and Southern Europe) and two physics packages (a basic and improved linear physics package) in the adjoint computations. Each experiment included a 3-month summer and winter period.

Sensitivities have been produced at all model levels, ranging from the surface up to 0.1 hPa, from optimizing a diagnostic function in 3 iterations, see section 2.1. We produced climatologies of sensitivities only for the first and third iteration, *i.e.* the scaled gradient and key analysis errors respectively. In addition, perturbed forecasts up to 10 days were produced from analyses perturbed with the key analysis errors. These forecasts have been used in the previous chapter to validate the experimental configuration, in section 2.5 and will be used in this chapter to assess the impact of the improved physics package against the basic physics. All results have been archived in the Meteorological Archiving and Retrieval System (MARS) archive at ECMWF. Retrieval of archived data is described in appendix A.

Dedicated tools have been developed with the MetView visualization package to retrieve data from MARS, to post-process the data and to plot the results. These tools include plotting of climatology maps of sensitive areas at individual model levels and integrated in the vertical, time diagrams and vertical cross sections. For each of the four experiments and for both winter and summer period we produced i) maps of sensitive areas for temperature, wind, vorticity, divergence and total energy at 250 hPa, 500 hPa and 1000 hPa and for surface pressure to determine the spatial distribution of sensitivities at these levels, ii) time diagrams of temperature, vorticity, divergence, geopotential height and total energy forecast errors at 250, 500 and 1000 hPa and of surface pressure to quantify the impact of perturbed analyses on forecasts. Besides maps at individual levels, we integrated sensitivities in the vertical to provide climatology maps of the lower, medium, upper and complete troposphere. Finally, we produced vertical cross sections of sensitivities for temperature, wind, vorticity, divergence and total energy to assess their vertical extend.

Considering four experiments and two time periods we produced a large amount of plots. They have all been archived and may be retrieved from the ECMWF File System (ECFS) as described in appendix A. For this report, we filtered the most relevant results. Section 4.2 discusses the main differences between climatology maps from scaled gradients and key analysis errors. Next, we assess the impact of the improved physics package against basic physics by considering total energy, average scores of perturbed forecasts and climatology maps in section 4.3. Based on the results of these two sections, we present the most relevant climatologies in section 4.4. The results are evaluated and the conclusions should provide the EUCOS community with information suggesting where to operate new observation instruments in the future.

4.2 Scaled gradients vs. key analysis errors

This section discusses the main differences between climatology maps of scaled gradients and key analysis errors. Climatology maps are produced at model levels by averaging sensitivity fields over the 3-month period (either winter or summer) as follows. Define $S_\alpha(i,j,t,m)$ the archived sensitivity field value of parameter α at grid point (i,j), model level m and day t and $c_\alpha(i,j,m)$ the climatology map value at grid point (i,j) and model level m, then

$$c_\alpha(i,j,m) = \frac{1}{T}\sum_{t=1}^{T} S_\alpha(i,j,t,m) \tag{4.1}$$

The summation is over the complete T days winter or summer period. We produced maps at model levels corresponding to 250, 500 and 1000 hPa for temperature, wind, vorticity and divergence and for surface pressure, all for the Northern and Southern Europe target areas.

Generally, the location of sensitive areas is very similar for scaled gradients and key analysis errors. An exception is displayed in Fig. 4.1. It shows the summer climatologies of scaled gradients and key analysis errors for temperature at 500 hPa. The target area is Southern Europe. Note the different scaling of the colour contours in both plots. Here, we are not interested in the sensitivity amplitudes, which is roughly a factor 3 larger for key analysis errors, but merely on their location. Both figures in Fig. 4.1 show sensitive areas west of the North African coast at (20W-32N), over the North African continent at (8W-28N) and at south Spain. Note the sensitive area south-west of Spain present in Fig. 4.1b, which is not present in Fig. 4.1a. Moreover, sensitive areas in the Mediterranean, Gulf of Biscay and east of France are more pronounced in Fig. 4.1b.

Based on climatology maps only it is hard to adjudge more confidence to climatologies of either scaled gradients or key analysis errors. Individual days within the summer period should be investigated and sensitivities should be related to the specific meteorological situation. This is beyond the scope of this report. However, climatology maps of both sensitivities do not contradict and generally show sensitive areas at the same locations. In the remainder of this report we concentrate on key analysis errors for which perturbed forecasts are available, hence an objective measure to assess their impact on 48-hour forecasts. A theoretical argument in favour of using key analysis errors is the closer correspondence of evolved key analysis errors to forecast errors showing that key analysis errors are more realistically projecting on the full analysis error, see [6].

4.3 Basic vs. improved physics

As explained in Chapter 2, we extended the ECMWF sensitivity configuration to include the improved linear physics package in the adjoint computations. This section assesses the impact of this extension by verifying total energy forecast error reduction, perturbed forecast scores and sensitivity maps against those from the ECMWF operational simplified physics package. Fig. 4.2 shows the total energy forecast error reduction from minimizing the diagnostic function with total energy norm, Eqs. (2.1) and (2.2), in 3 iterations. The achieved reduction is between 40 and 50%, but slightly larger for the basic physics package. This suggests that inclusion of the improved physics package in the sensitivity computations requires more iterations to achieve similar forecast error reduction as with basic physics. The figures also show that the curves relating to basic and improved physics mainly overlap and only differ significantly for a small number of days. For these cases, it would be interesting to study in more detail the impact of the iteration number and the particular meteorological situation.

From Fig. 4.2 we notice a large reduction of total energy forecast error for forecasts worse than average, implying that potentially forecasts can be improved significantly through better observing and analysing the sensitive areas. Besides a large reduction of the peaks, the curves of the reduced total energy errors are much smoother than those of the initial forecast error. This agrees with the

a)

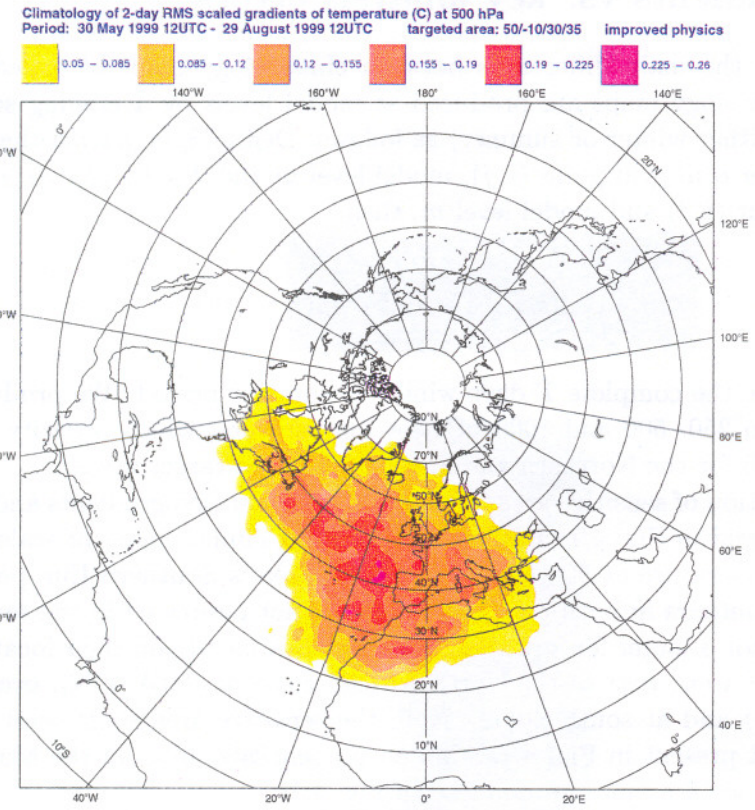

b)

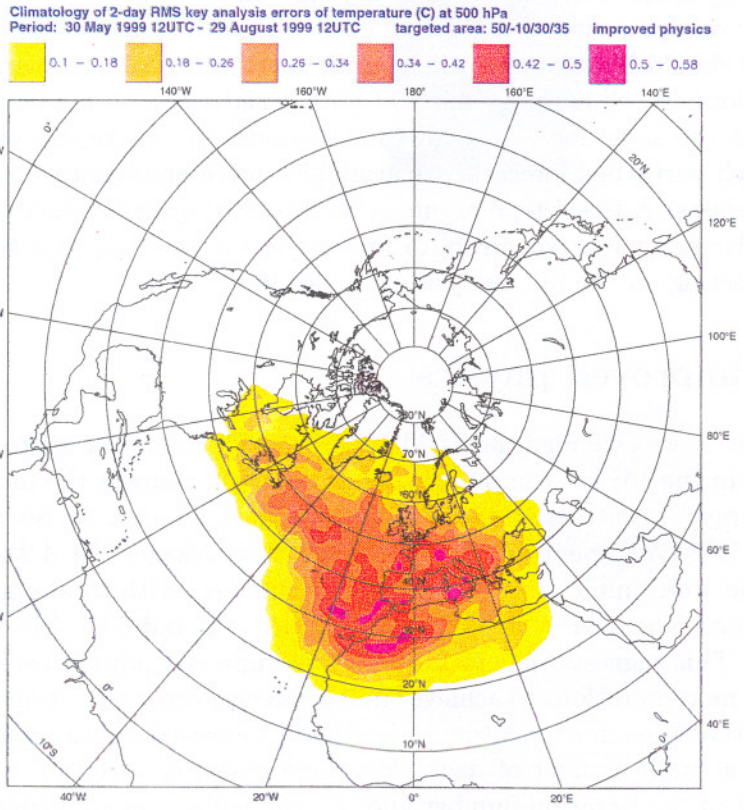

Figure 4.1: Climatologies of sensitive areas for temperature at 500 hPa in the summer period. a) Scaled gradients and b) key analysis errors. The target area is Southern Europe.

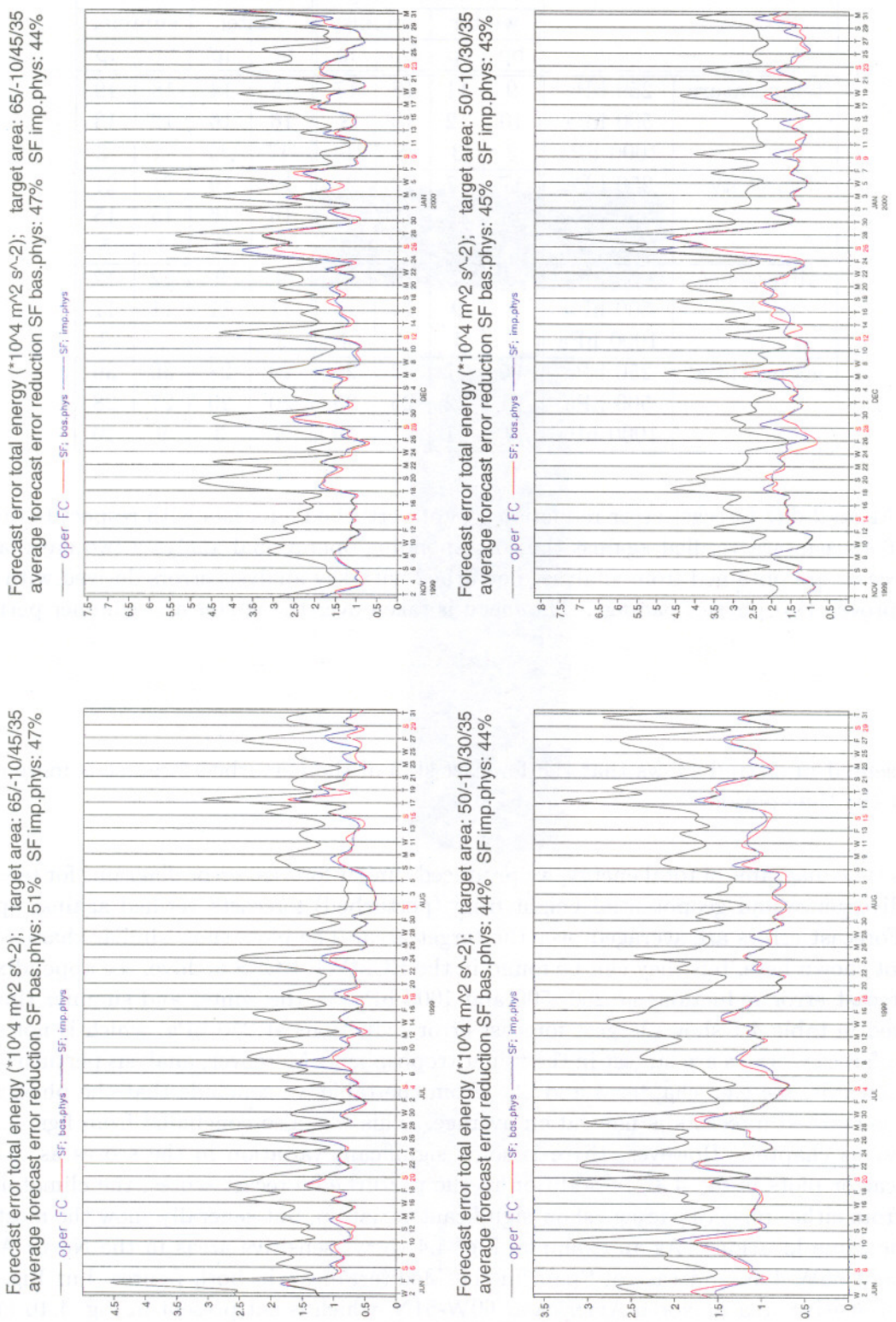

Figure 4.2: Time diagrams of 2-day total energy forecast error integrated over the target area. Black lines denote the total energy of the initial operational forecast errors, the red and blue lines correspond to minimized forecast errors using the basic and improved physics package respectively. Upper-left: Northern Europe winter, upper-right: Southern Europe winter, lower-left: Northern Europe summer and lower-right: Southern Europe summer.

		Northern Europe				Southern Europe			
		winter		summer		winter		summer	
		bp	ip	bp	ip	bp	ip	bp	ip
temperature	250 hPa	9	11	18	17	15	14	18	19
	500 hPa	10	12	10	8	16	16	12	13
	1000 hPa	3	3	5	6	-17	-17	-4	-3
vorticity	250 hPa	17	17	22	21	19	19	21	21
	500 hPa	14	15	16	15	16	16	15	15
	1000 hPa	10	10	8	8	2	2	4	5
divergence	250 hPa	6	7	15	15	9	9	12	12
	500 hPa	8	9	14	15	11	11	11	11
	1000 hPa	0	1	4	4	2	2	1	3
geopotential	250 hPa	25	27	28	26	29	28	36	36
	500 hPa	21	22	26	25	20	20	27	28
	1000 hPa	9	11	17	16	4	3	9	10

Table 4.1: Mean 2-day forecast error reduction (%) of perturbed forecasts with respect to operational forecasts. Forecasts are verified against the corresponding operational analyses two days later. Perturbed forecasts are obtained from analyses perturbed with key analysis errors derived with the basic (bp) or improved (ip) physics package. The mean is taken over the winter and summer periods.

results presented in [2] and shows that the forecast skill of the perturbed forecast is more consistent throughout the time period.

Besides time diagrams of total energy, we produced similar forecast error diagrams for temperature, vorticity, divergence and geopotential height from (perturbed) forecasts verified against operational analyses. Forecast errors are averaged over the target area. The plots show similar characteristics as Fig. 4.2 (not shown here, but they can be found in the ECMWF ECFS archive, see appendix A). The average forecast error reductions at 250, 500 and 1000 hPa for the winter and summer time periods are displayed in table 4.1 shows largest forecast error reductions at 250 hPa, which is not surprising since initial forecast errors are largest in the upper troposphere. Moreover, analysis perturbations tend to evolve upwards, see e.g. chapter 3 and [2]. From the table we conclude that the physics package impact on perturbed forecasts is neutral on average. This was also concluded from figs. 2.7 and 2.8 of the previous chapter. However, there is some significant variation in the scores as can be seen from the scatter plots in fig. 4.3. In addition to the perturbed forecast scores, the climatology maps produced from either physics package show significant variation, but generally show the most sensitive areas at the same locations. As an example, Fig. 4.4 shows sensitive areas in the North Atlantic at 30W-57N and 55W-43N and east of Spain in the Mediterranean in both figures, but Fig. 4.4a also has a clear sensitive area in North America at 60W-51N, which is not present in Fig. 4.4b From these figures we conclude that there is an impact of the improved linear physics package, but it is hard to judge whether corresponding sensitivies are more reliable than those produced with the basic physics package based on perturbed forecast scores only. As in the previous section this requires an extensive study of forecast errors, the particular meteorological conditions and produced sensitivities on a daily basis which is beyond the scope of this study. For the production of the climatologies in the next section we will use sensitivities produced with the improved physics package because they are expected too be more physically reliable.

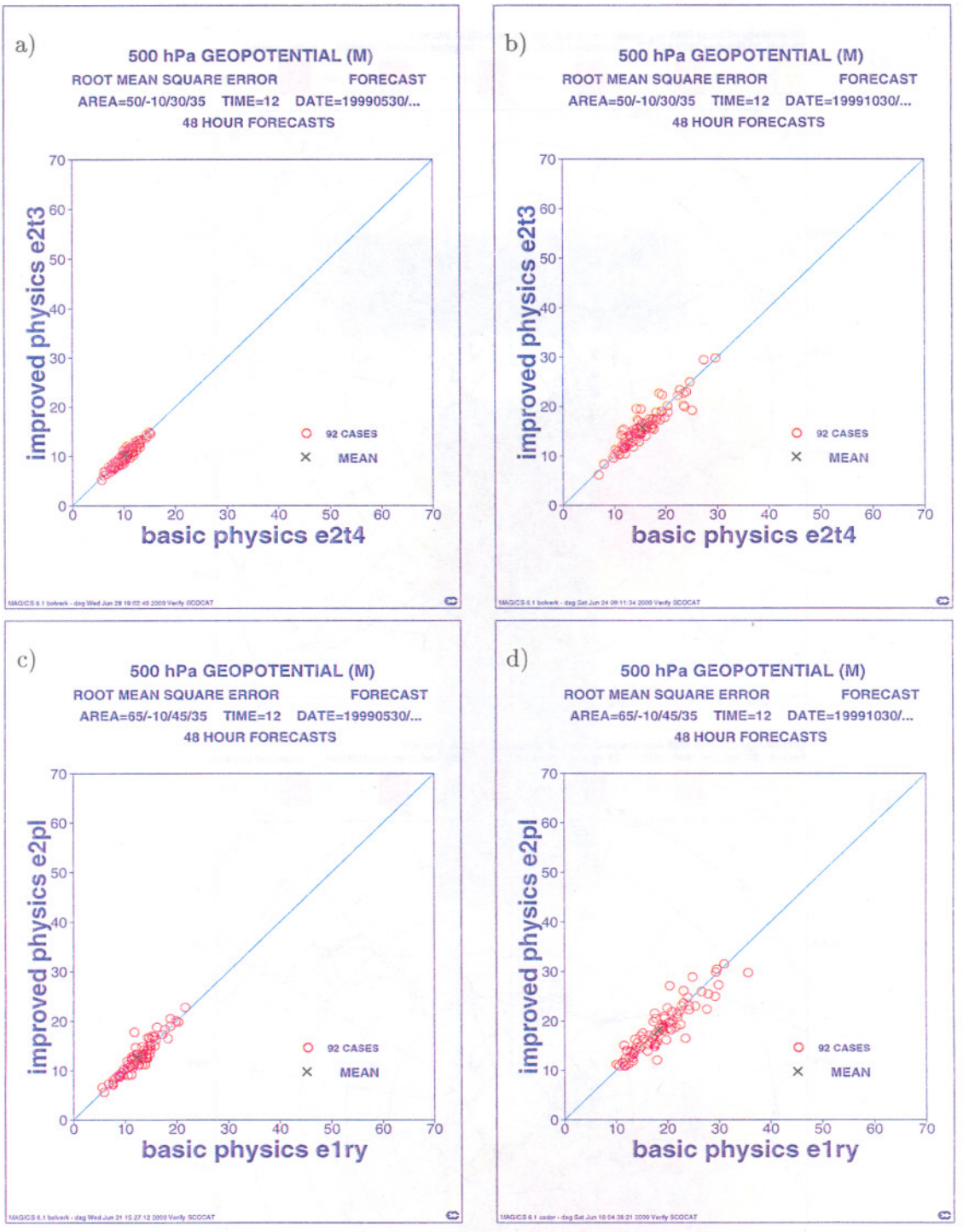

Figure 4.3: Scatter plot of perturbed forecast 500 hPa geopotential height RMSE. Perturbed forecasts are obtained from key analysis errors produced with either improved physics (vertical axis) or basic physics (horizontal axis). a) Southern Europe, summer period, b) Southern Europe, winter period, c) Northern Europe, summer period and d) Northern Europe, winter period.

4.4 Climatologies of sensitive areas

We produced climatology maps of sensitive areas for individual pressure levels at 1000, 500 and 250 hPa. These maps are obtained from averaging over either the winter or summer period. The results are

a)

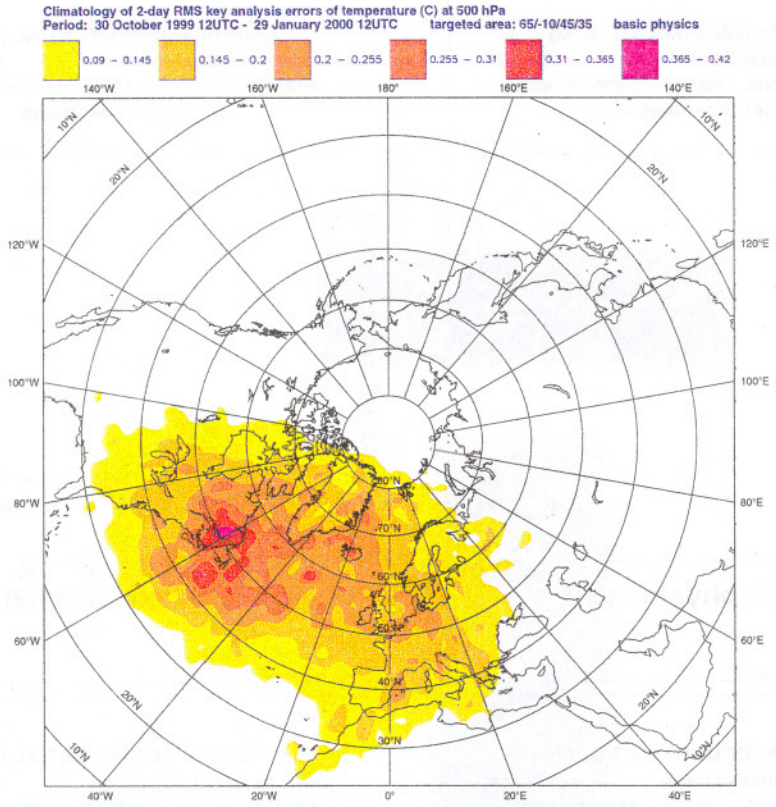

b)

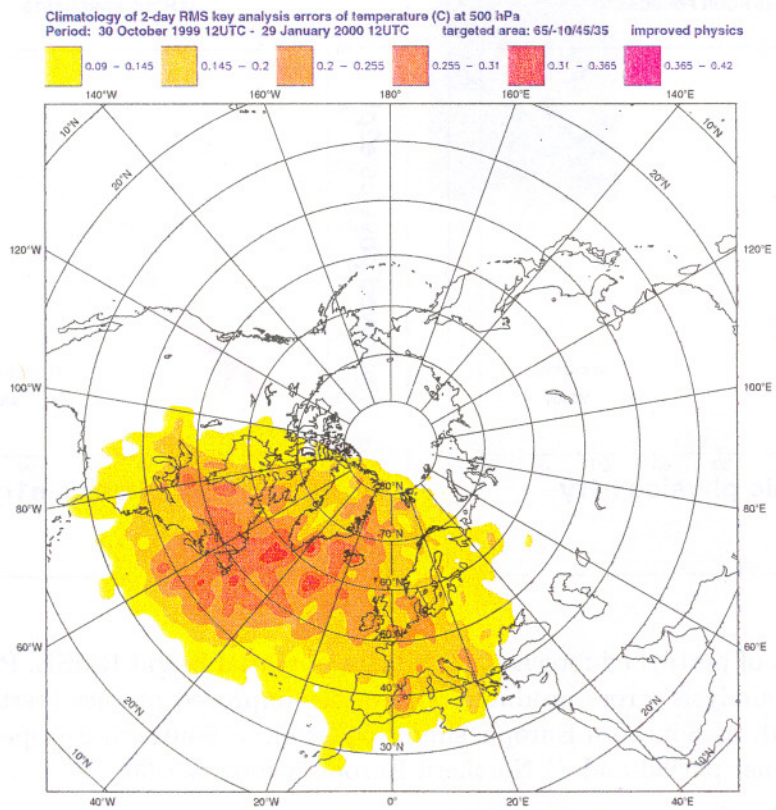

Figure 4.4: Climatology maps of sensitive areas for temperature at 500 hPa in the winter period produced with a) basic physics and b) improved physics. The target area is Northern Europe. Note the sensitive area at 60W-51N present in a) but not very pronounced in b).

archived, see appendix A. Besides, we integrated the sensitivities in the vertical. We considered four atmospheric layers representing the lower, medium, upper and the complete troposphere respectively. For these layers, we produced climatology maps for temperature, wind, surface pressure and total energy. In this report we only present maps of the latter which comprises temperature, wind and surface pressure according to Eq. (2.2). Climatology maps of temperature, wind and surface pressure have been archived, see appendix A. Climatology maps of total energy have been produced as follows. We retrieve archived fields of key analysis errors for temperature S_T and wind components S_u and S_v at all model levels m and the logarithm of surface pressure S_{lnps}. Each field consists of grid point positions (i, j). Total energy sensitivity S_{TE} at position (i, j) at level m and day t is defined as

$$S^2_{TE}(i,j,t,m) = S^2_u(i,j,t,m) + S^2_v(i,j,t,m) + R_a T_r S^2_{lnps}(i,j,t,m) + \frac{C_p}{T_r} S^2_T(i,j,t,m) \tag{4.2}$$

The unit of S_{TE} is (m/s). The constants in Eq. (4.2) are similar as in Eq. (2.2). Root mean total energy (RMTE) climatology maps for atmospheric layers are produced by first averaging total energy key analysis errors in time to produce climatology maps for individual model levels, similar as in eq. (4.1). Next, these maps are integrated vertically through weighted averaging over model levels, the weight determined by the pressure layer thickness. In formulae:

$$\mathrm{IRMTE}(i,j) = \frac{1}{\sum_m \delta p(m)} \sum_m \left\{ \sqrt{\frac{1}{T} \sum_{t=1}^{T} S^2_{TE}(i,j,t,m)} \right\} \delta p(m) \tag{4.3}$$

Where IRMTE denotes the integrated root mean total energy sensitivity field. The expression between braces represents the RMTE sensitivity field. The summation between braces is over the time period T, which is 92 days for both the winter and summer period. The vertical integration is performed by a summation over model levels m outside the braces. Climatologies at individual levels are weighted with the layer pressure thickness, $p(m)$. For the lower, medium, upper and complete troposphere the summation extends from i) the surface to 700 hPa, ii) 700 hPa to 350 hPa, iii) 350 hPa to 200 hPa and iv) from the surface to 200 hPa respectively.

In this section we present only IRMTE climatology maps that are integrated over the troposphere from the surface to 200 hPa. Climatology maps for the lower, medium and upper troposphere are found in appendix B. These maps provide the geographical location of sensitive areas. Climatology maps at individual model levels also serve as input to produce vertical cross sections. For this purpose the climatology maps are averaged in North-South direction between two latitude values to produce the mean amplitude of sensitivities as a function of longitude. Performing this operation for all model levels provides a picture of the most sensitive atmospheric layers.

Figs. 4.5, 4.6, 4.7 and 4.8 show climatology maps of the IRMTE and vertical cross sections of the RMTE for the two EUCOS target areas and the winter and summer periods. The geographical locations of sensitive areas agree well with the mean Westerly flow which is stronger in the winter than in summer. As a result, sensitive areas are closer the EUCOS target areas in summer than in winter. Sensitive areas for Southern Europe are more Southernly positioned and extend to Northern Africa. For all four climatologies sensitive areas are found in the band 40N-60N,60W-30E, which covers part of the North American continent, the Northern Atlantic and large parts of the European continent. Most sensitive areas for both the Northern and Southern Europe target areas are found in the Northern Atlantic in the center between North America and Europe for both winter and summer periods, and for the North American coast (summer and winter), Greenland (mainly winter) and the European coast (summer and winter). The Mediterranean and the North African coast and continent are sensitive areas for the Southern Europe (SE) target area in both winter and summer periods.

From the vertical cross sections it follows that sensitivities are strongest in the mid-troposphere between 700 and 400 hPa, at higher pressure values in the winter.

Northern Europe, summer, integrated total energy

a)

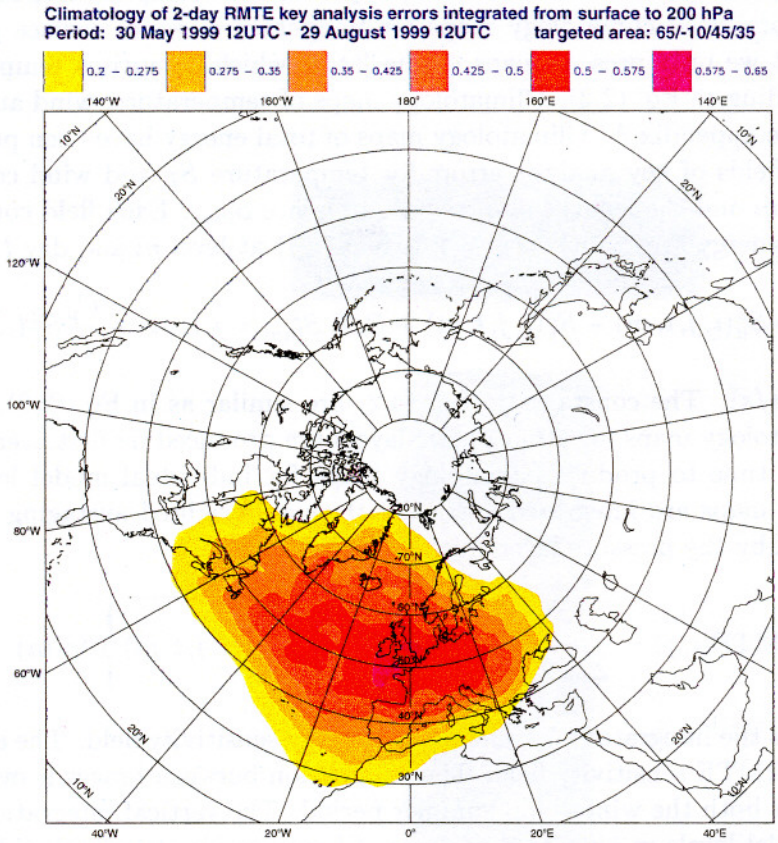

b)

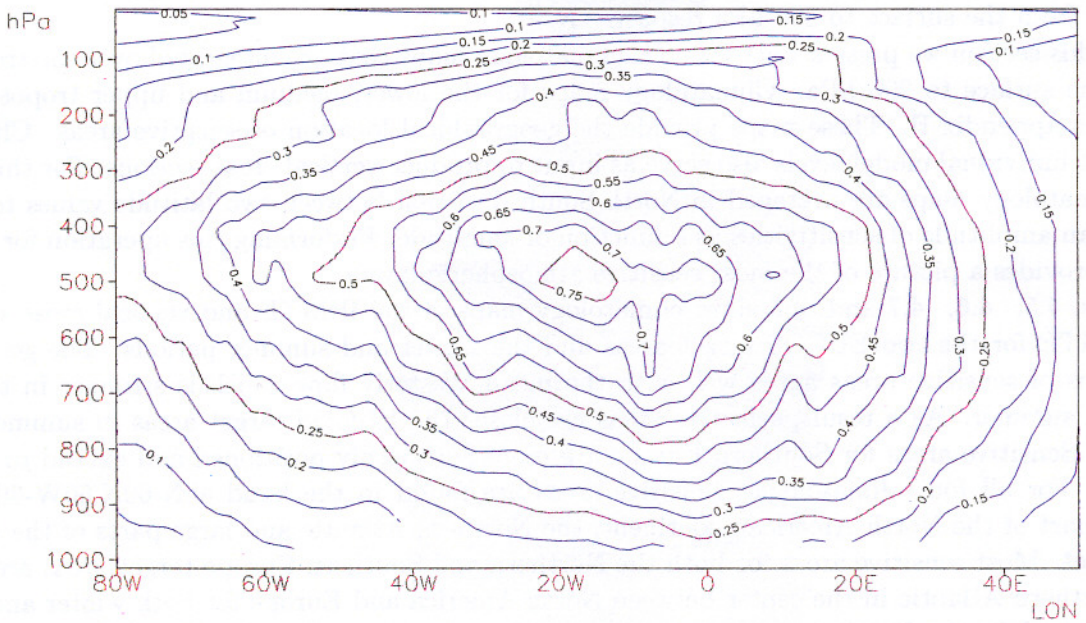

Figure 4.5: Northern Europe summer period climatology of IRMTE (see text) sensitive areas. a) Sensitivities are integrated in the vertical from the surface to 200hPa. b) Vertical cross section of RMTE. Single model level climatology maps are averaged between 35N and 75N. The contour interval is 0.05 m/s.

Northern Europe, winter, integrated total energy

a)

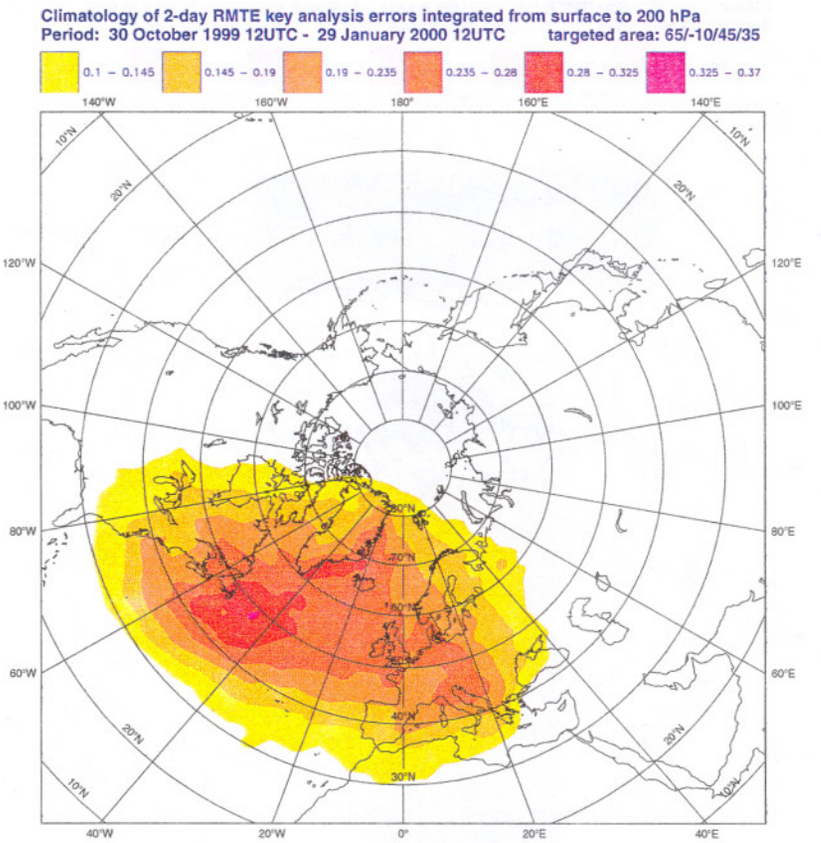

b)

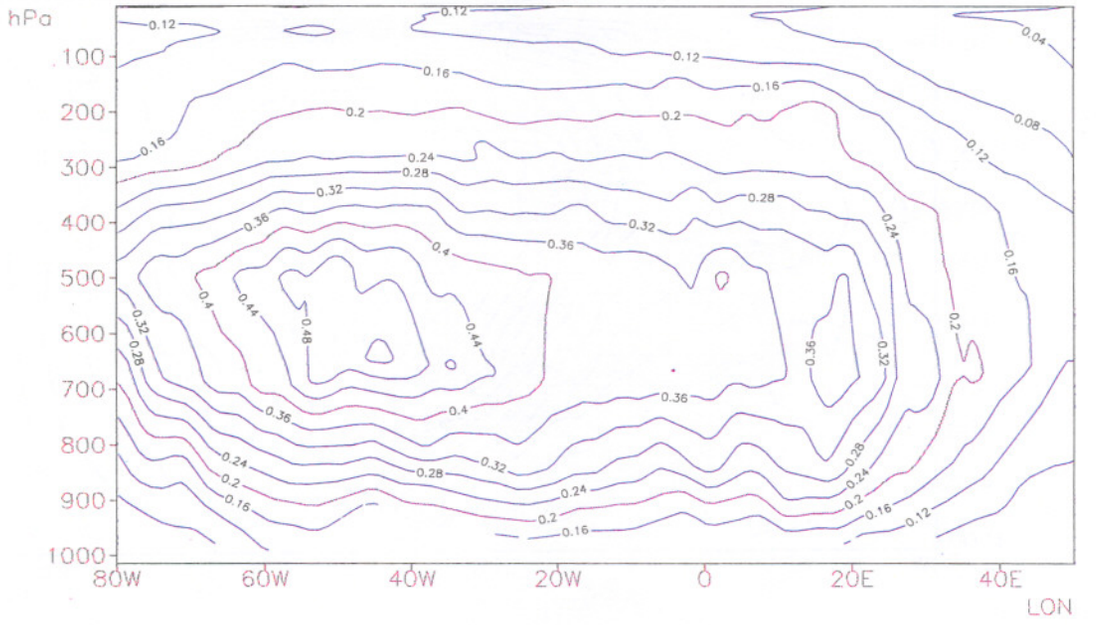

Figure 4.6: Northern Europe winter period climatology of IRMTE sensitive areas. a) Sensitivities are integrated in the vertical from the surface to 200hPa. b) Vertical cross section of RMTE. Single model level climatology maps are averaged between 35N and 75N. The contour interval is 0.04 m/s.

Southern Europe, summer, integrated total energy

a)

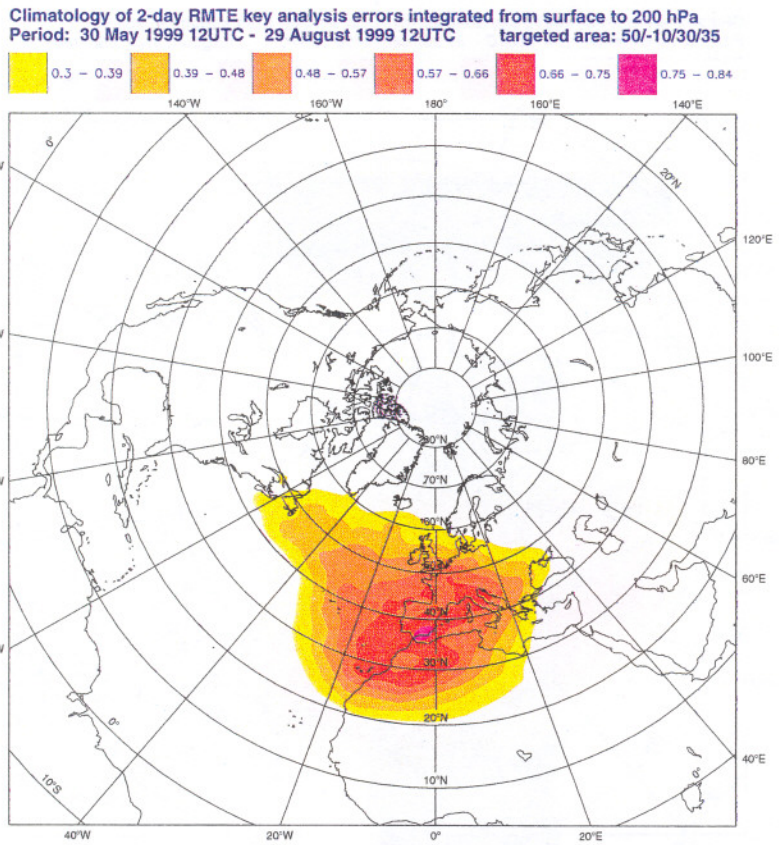

b)

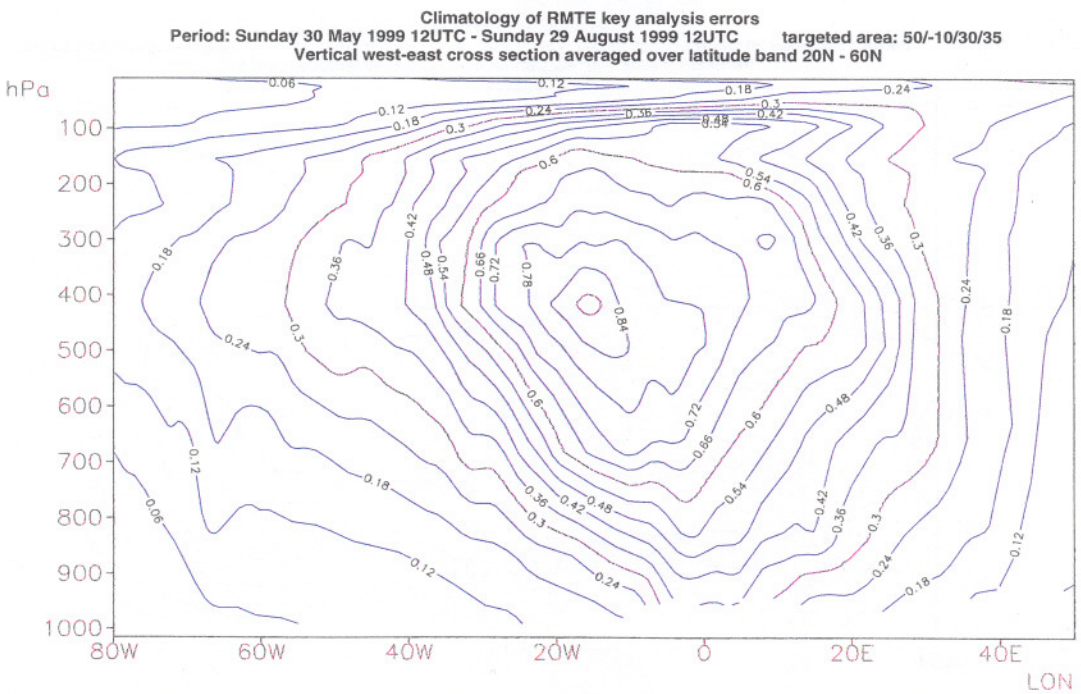

Figure 4.7: Southern Europe summer period climatology of IRMTE sensitive areas. a) Sensitivities are integrated in the vertical from the surface to 200hPa. b) Vertical cross section of RMTE. Single model level climatology maps are averaged between 20N and 60N. The contour interval is 0.06 m/s.

Southern Europe, winter, integrated total energy

a)

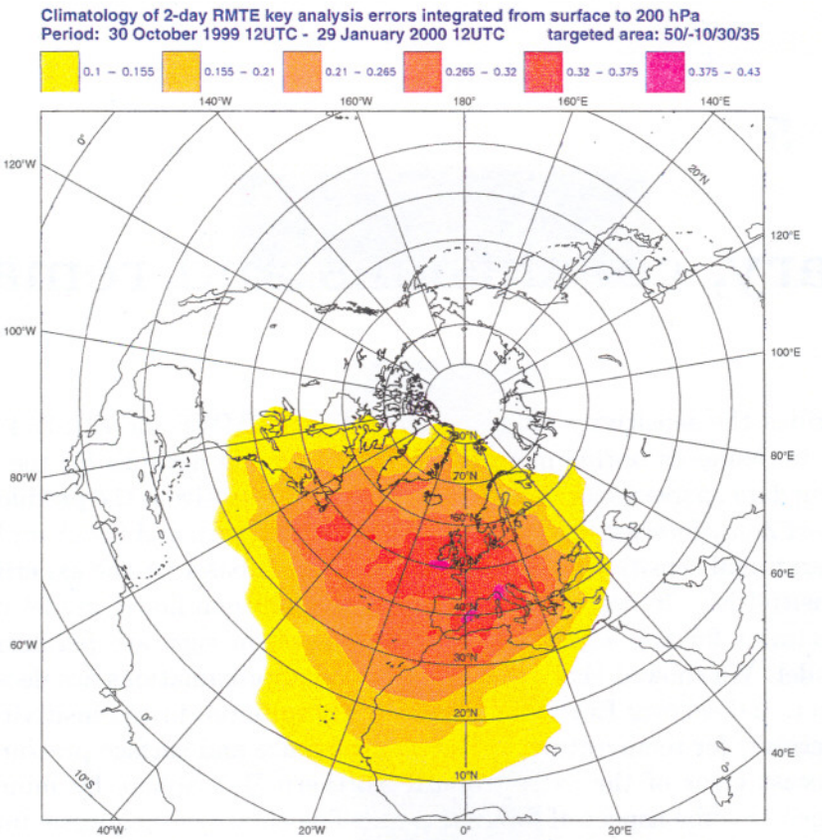

b)

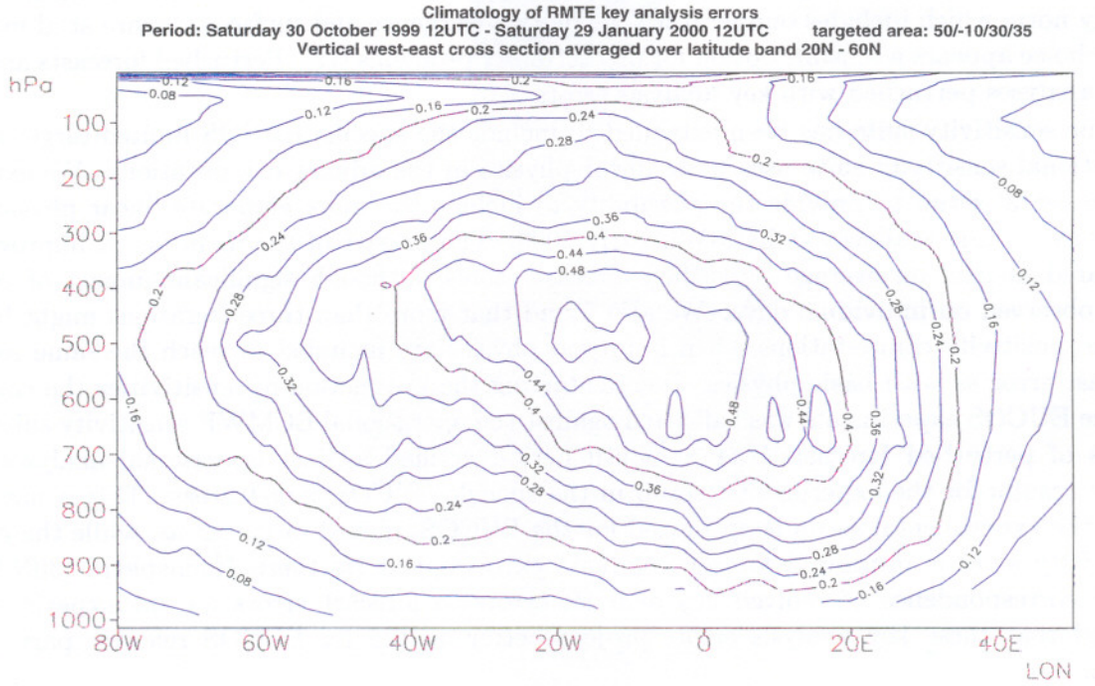

Figure 4.8: Southern Europe winter period climatology of IRMTE sensitive areas. a) Sensitivities are integrated in the vertical from the surface to 200hPa. b) Vertical cross section of RMTE. Single model level climatology maps are averaged between 20N and 60N. The contour interval is 0.04 m/s.

Chapter 5

Summary, conclusions and remarks

This report describes the sensitivity study performed at ECMWF for EUMETNET as part of the EUCOS program to define an optimum ground based observing network for the European continent and its surrounding data sparse areas. The sensitivity study objective is the production of climatologies for sensitive areas of 2-day forecast error over the EUCOS Northern and Southern Europe target areas. The ECMWF operational sensitivity suite has been used as a basis for the experimental setup for the production of sensitivities. It uses a low resolution T63L60 non-linear model using full physics to provide the trajectories for the adjoint integrations, which in turn are performed using a T63L60 tangent linear model. We showed that the low resolution approximations are decent enough for short range forecasts up to 2 days over Europe. The sensitivity suite produces sensitivities (scaled gradients and key analysis errors) for temperature, vorticity, divergence and surface pressure at all model levels for the 2-day forecast error of the extra-tropical Northern Hemisphere by minimizing a diagnostic function that describes some aspect of forecast error. The choice of diagnostic function is not unique and might depend on the specific forecast error aspect under study. In this study we used the total energy norm which includes temperature, vorticity, divergence and surface pressure at al model levels. This choice appears a sensible option for predictibility problems [12]. Perturbed forecasts are produced from analyses perturbed with key analysis errors.

The sensitivity suite has been extended to include the specific EUCOS limited target areas. The operational sensitivity suite uses basic linear physics in the adjoint computations. We extended the experimental setup to provide the possibility to include the more elaborate linear physics package, that has become available at ECMWF early 2000. The impact of the inclusion of improved physics appeared neutral on average perturbed forecast scores, although significant impact of physics has been observed on individual days. We also found that more than three iterations might be required in the sensitivity computations when improved physics are included to reach the same reduction of forecast error as with basic physics. Before starting the production of sensitivities the configuration for the EUCOS experiments was validated against the operational ECMWF sensitivity suite. Average scores of perturbed forecasts over a month period verified against operational analyses produced better results for the experimental setup in the specific EUCOS target areas. This is not surprising since the experimental setup is optimized for the EUCOS limited target areas, while the operational sensitivity suite is optimized for the complete extratropical Northern Hemisphere (30N-90N). The closer correspondence of evolved key analysis errors to forecast errors for the experimental setup showed that these key analysis errors project better on the for EUCOS relevant part of analysis errors.

Four experiments have been performed, specified by the Northern and Southern Europe target areas and the use of basic and improved physics in the adjoint computations. All results, mainly sensitivities and perturbed forecasts, have been archived in MARS. Data retrieval of these experiments is described in appendix A.

We first discussed some interesting individual cases in chapter 3 before discussing the production of climatologies of sensitive areas in chapter 4. The case studies showed that errors in the operational 2-day forecast can be explained partly by initial errors in the operational analysis. Evolution of key analysis errors reduced the forecast error significantly. For the Christmas case of 27 december 1999 we showed that it is important to capture the interesting forecast error feature completely in the target area to produce correct perturbations for the initial analysis. For this particular case the operational sensitivity suite, optimized to produce sensitivites for the complete Northern Hemisphere, produced key analysis errors that projected better on the analysis error and evolved to correct the 2-day forecast error at the correct location. The sensitive areas for this case were mainly located in the Northern Atlantic near the North American coast.

The second case in the summer period on 3 June 1999 described the correction of a wrongly positioned trough at 500 hPa in the Channel. We found sensitive areas located both in the Northern Atlantic and parts of Northern Africa. Their evolution corrected most of the forecast error. It should be stressed that the main goal of this study was not to explain forecast errors for extreme individual cases but to produce sensitivities for the complete European target areas.

Chapter 4 discussed the production of climatologies of sensitive areas. We first assessed the use of scaled gradients versus key analysis errors and the use of sensitivities produced with either basic or improved physics in the adjoint computations. We adjudged key analysis errors produced with the improved physics package as most reliable input for the climatology production. Next, we discussed the production of climatologies. We produced climatology maps for temperature and wind at individual pressure levels on 250, 500 and 1000 hPa and for surface pressure by averaging sensitivity fields in time. Next, these climatology maps were integrated in the vertical, after proper weighting with pressure layer thickness, to produce climatology maps representing the lower, medium, upper and complete troposphere. These resulting maps are not presented in this report but have been archived at ECMWF, see appendix A.

To present a small representative set of climatology maps in this report, we introduced the integrated root mean total energy (IRMTE) that combines sensitivities for temperature, the wind vector and surface pressure in a physical way, similar as in the total energy norm. As for the other parameters, climatology maps of IRMTE were produced first at individual levels and next integrated in the vertical. In chapter 4 we presented climatology maps of IRMTE, integrated over the complete troposphere from the surface to 200 hPa and vertical cross sections. Appendix B contains climatology maps that represent IRMTE sensitivities for the lower, medium and upper troposphere.

From the climatologies it was concluded that sensitive areas for 2-day forecast error in the two European target areas are located in the band 40N-60N,60W-30E, which covers part of the North American continent, the Northern Atlantic and large parts of the European continent. Most intense sensitive areas for both the Northern and Southern Europe target areas are found in the Northern Atlantic in the center between North America and Europe for both winter and summer periods, and for the North American coast (summer and winter), Greenland (mainly winter) and the European coast (summer and winter). The Mediterranean and the North African coast and continent are sensitive areas for the Southern Europe (SE) target area in both winter and summer periods. The vertical cross sections showed that sensitive areas are most intense in the mid-tropospere between 700 and 400 hPa. We note that the produced climatologies are based on a single winter and summer period only. Year-to-year variations of the mean flow might produce different climatologies for other periods.

The final step is to translate the produced climatology maps and vertical cross sections of key analysis errors to a strategy of where to operate and what kind of additional observations. This is not a trivial step. Ideally, additional observations should perturb the initial analysis very close to the key analysis errors. Obviously, observations should be targeted at least close to sensitive areas, but the number of required observations and their geographical location to describe the most

sensitive features very much depends on the underlying data assimilation system. Most sensitivity studies do not involve any considerations of the characteristics of the data assimilation system. In particular, the interaction of additional observations with the background field, other observations and the background and observation error statistics are ignored. Consequently, the location of sensitive areas does not necessarily coincide with the area where to perform targeted observations as experienced from the FASTEX and NORPEX observation-targeting experiments [11]. The method does not tell us whether produced sensitivities are likely to happen in practice. From our results it follows that perturbations of the initial analysis in the mid-troposphere have a larger impact on the diagnostic function than equally large perturbations in the upper troposphere. However, larger errors might be more likely in e.g. the jet than at lower levels. The sensitivities found should therefore be normalized by the relative uncertainty in the initial conditions. [3, 4].

The EUMETNET study of Martin Leutbecher showed that "smart" sampling of the sensitive area for the Christmas 1999 case required about 40 additional soundings to the assimilation system to describe the main sensitive features reasonably well. On the other hand, it was shown that too many additional data in a small area should be avoided. Additional data in well observed areas might not be very informative. Presumably, data will always be informative in data sparse areas. However, data sparsity is not well defined in practice and depends e.g. from the specific meteorological situation, e.g. satellite data might not be able to penetrate cloudy scenes hence obscuring the lower atmosphere. Further studies are required to study the correlation of sensitive areas with e.g. cloudy scenes.

The archived sensitivities might prove a useful source of information for future studies to assess the potential impact of new observation systems for numerical weather prediction, e.g. to assess capability of future spaceborne Doppler wind lidar systems to observe sensitive areas.

From sensitivity studies to observation planning

(by F. Bouttier)

The forecast error sensitivity studies presented by G.-J. Marseille give a convincing picture of the areas where, in average, an improvement of the analysis will improve the short-range forecast performance over Europe. These areas can be summarized as follows:

- The Atlantic North of 30N up to and including Greenland, Spitzbergen and the North Pole,
- The USA and Canada East of 100W,
- Europe itself
- The Mediterranean sea
- NorthWest Africa including Morocco, Algeria, Senegal and Cabo Verde.

The most sensitive areas are the 20N-60N latitude band from the American East Coast to the Alps, the area between Greenland and Iceland, and the area between Madeira, the Canaries and the Moroccan Atlas mountains.

There are variations depending on season, target area and parameter, but the broad features of the geographical distribution remain the same. It suggests that this distribution is rather robust. The sample included many different weather patterns and it is not believed that the average would have been significantly different if another year or season had been selected. In the vertical, the main sensitivity is between 300hPa and 700hPa; the sensitivities are much weaker above the tropopause and near the surface.

An improvement of the analysis in these sensitive areas and levels will improve the 2-day forecasts in average. There are, however, some restrictions on the conclusions that can be drawn:

- adding observations in these areas will not necessarily result in an improvement of the forecasts. This can only be obtained if the areas are not already well observed and if the added observations are abundant and with a good quality.
- there is no indication that the improvement will happen in all types of weather situations (e.g. that storm forecasting will be improved).
- due to the statistical nature of the analysis schemes, optimal deployment of additional observations will not result in a systematic forecast improvement. The improvement can only be expected in average over a sample of forecasts.
- if a sensitive area is not well observed, or if the analysis system is making poor use of observations in this area, the forecast will be sensitive to improvements in the background fields, i.e. to observations further upstream of the sensitive area.
- the plots emphasize areas with a strong spatial density of sensitivity, but the forecasts can also be improved by changing the analysis at larger scales and with a smaller amplitude.

A precise recommendation for observation deployment would need to include indications on which atmospheric parameter to observe, with which geometry (single level, vertical average or vertical profile) and on which scales. It would not be honest to be as specific as this, because of the approximations involved in the study and in the interpretation of the results, notably:

- the linearization hypothesis and the perfect model hypothesis,
- the assumptions that analysis systems make about the scale of the forecast errors and their multivariate relationships,
- the fact that many important analysis errors develop over some time in the data assimilation process, and their correction by a single analysis after they have amplified may require an unfeasibly expensive observing system and data assimilation scheme.

Moreover, the recommendation of one observation type over another can only be made with consideration of the economical cost of each option, which is outside the scope of this study. Finally, the usefulness of some observing systems (such as satellite radiances or Lidar winds) will be sensitive to their actual information content, which cannot be accurately predicted, as past experience with satellite data has shown.

Based on the existing expertise on data assimilation, this study leads to suggesting the following subjective recommendations for deploying new observations:

- the geographical distribution should attempt to sample the abovementioned sensitive areas as well as possible.
- the vertical distribution should concentrate on the mid-troposphere. Observations above the tropopause and at low levels seem less useful. Note that the tropopause itself is already rather well sampled by flight-level aircraft reports, and that surface pressure information does provide information about the mid-troposphere because of the multivariate coupling in analysis schemes.
- Looking at the most sensitive areas in individual cases, the scale of the sensitive structures is very small in the horizontal (as small as the resolution of the model used in this study) and of the order of 50hPa in the vertical. Given the limitations in the effective resolution of current analysis systems, the marginal usefulness of additional observations would decrease in areas where the existing observing network has reached a sampling resolution of 50hPa in the vertical and 100km in the horizontal.
- For additional observations to have a significant impact on the analysis quality, their precision must be better than the background forecast errors. This is usually true over the oceans for in-situ upper-level data, but not always for low-level or remote-sensed data.
- The adjoint method used in this study does not account for the synoptic impact of errors in (notably) convection and surface fluxes. It must be understood that analysis errors with the structures considered in this study can easily be generated in an assimilation system by a slow growth of errors due to the modelling of these phenomena. Operational experience has shown that errors in convective areas often cause temperature and wind errors in the Gulf of Mexico, the East Coast of the USA, and the Atlantic region between Madeira and the Canary Islands. Low-level errors often cause mid-tropospheric errors over the whole of Canada, Greenland and the Arctic. Therefore, observations that improve the analysis of these features are expected to have an impact on the forecast performance, although the adjoint method cannot be used to depict the relevant areas, levels and parameters.

Appendix A

Data archiving

We sensitivities production included four experiments. All experiments produce scaled gradients and key analysis errors. The experiment identifiers are *e1ry*, *e2pl*, *e2t3* and *e2t4*. Their difference is in the target areas and used linear physics packages in the adjoint computations as follows:

- *e1ry*: Northern Europe target area, basic physics.
- *e2pl*: Northern Europe target area, improved physics.
- *e2t4*: Southern Europe target area, basic physics.
- *e2t3*: Southern Europe target area, improved physics.

An example of retrieving sensitivities from MARS (Meteorological ARchiving System) is displayed in Table A.1. The same setup is used to retrieve perturbed forecasts from MARS, with the following

				description
retrieve,				
	expver	=	e2pl,	experiment identifier
	class	=	'rd',	research department
	stream	=	'sf',	sensitivity forecast
	type	=	'sg',	data type scaled gradient
	param	=	't'/'vo'/'d'/'u'/'v'/'lnsp',	parameters
	date	=	19993010/to/20000129,	winter period
	step	=	0,	forecast step in hours
	levtype	=	'ml',	level type
	levelist	=	39,	list of pressure values
	diagnostic	=	1,	diagnostic value
	iteration	=	1/3,	scaled gradient (1)/ key analysis error (3)
	grid	=	1.5/1.5	grid size

Table A.1: Example of sensitivity retrieval from MARS. For experiment e2pl, fields of scaled gradients and key analysis errors are retrieved for temperature, vorticity, divergence, the horizontal wind components and the logarithm of surface pressure, all for model level 39 ($\sim$ 500 hPa for the 60 level model) and for the winter period ranging from 30 November 1999 until 29 January 2000. Note that the number of vertical levels in the operational ECMWF model is 50 in the summer 1999 period and 60 in the 1999/2000 winter period.

changes: type is set to 'sf', step is set to the desired forecast step ranging from 3 hours up to 240 hours, iteration should be set to 3, because only forecasts from analyses perturbed with key analysis errors

are produced. Sensitivities are only archived for model levels, perturbed forecasts also for pressure levels. For the latter, the level type could be set to 'pl' in the MARS retrieval.

We developed software for plotting sensitivity climatology maps and vertical cross sections of sensitivities as presented in chapter 4 and appendix B. The software and all plotting results are archived in the ECMWF File System (ECFS) in ec:/dag/eucos/climatologies/new. The archive contains the following postscript file results:

- clim_sens_*ll*_*exp1*_*exp2*_*p*.ps
  Single model level climatologies of sensitivities. *ll* denotes model level ranging from 1 (0.1 hPa) to 50 in summer and 60 in winter (about 1011 hPa), *exp1* the experiment with basic (named simplified in figure title) physics package and *exp2* the experiment with improved (named linear in figure title) physics package, *p* denotes the time period, i.e. *w* for winter and *s* for summer. The files contain climatology maps of both scaled gradients and key analysis errors for temperature and wind. For experiments *e1ry* and *e2pl* the target area is Northern Europe. For experiments *e2t4* and *e2t3* the target area is Southern Europe.

- clim_sens_*sp*_*exp1*_*exp2*_*p*.ps
  Climatologies of sensitivities for surface pressure. *sp* denotes surface pressure. The other extensions are as above.

- clim_sens_int_*exp*_*p*_*param*.ps
  Climatologies of key analysis errors integrated in the vertical. The files contain four plots representing the lower (surface to 700 hPa), medium (700 to 350 hPa), upper (350 to 200 hPa) and the whole tropospheric layer (surface to 200 hPa). *exp* denotes the experiment identifier, *p* the time period and *param* the metereorological parameter which is either *t* for temperature, *w* for wind vector, *vo* for vorticity and *d* for divergence.

- clim_xsection_TE*exp*_*p*.ps
  Vertical cross section climatologies of RMTE (root mean total energy) key analysis errors for experiment *exp* and period *p*.

- xsection_*exp*_*p*.ps
  Vertical cross section climatologies of RMSE key analysis errors of temperature, vorticity and divergence.

- xsection_wind_*exp*_*p*.ps
  Vertical cross section climatologies of RMSE key analysis errors of the wind vector.

- clim_sens_RMTE_*exp*_*p*.ps
  Climatology maps of RMTE key analysis errors integrated in the vertical. The files contain plots representing the lower, medium, upper and the whole tropospheric layer. *exp* denotes the experiment identifier, *p* the time period

Appendix B

Climatology maps of sensitive areas

Climatologies Northern Europe, summer

upper troposphere total energy

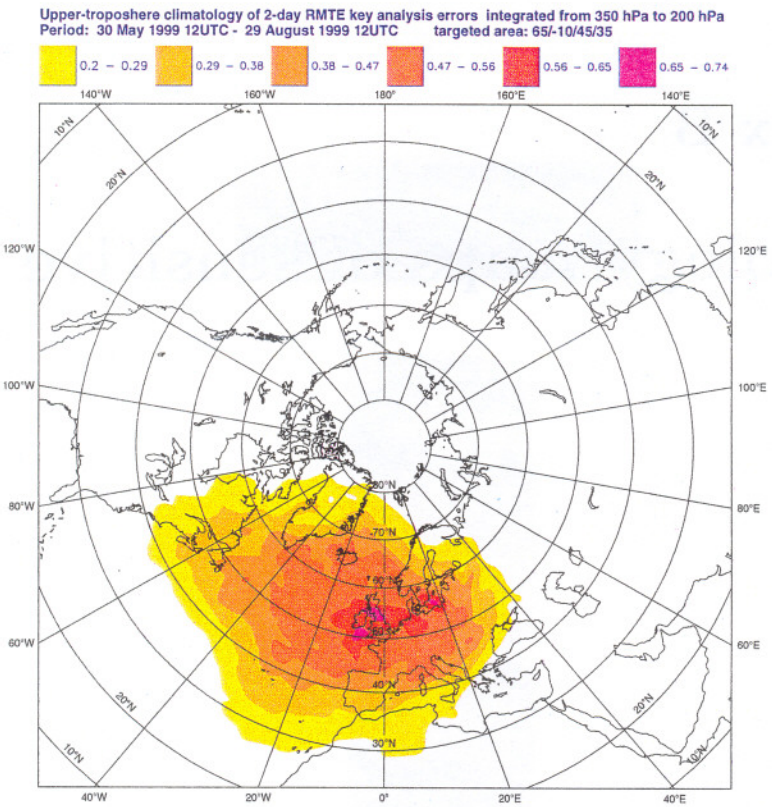

medium troposphere total energy

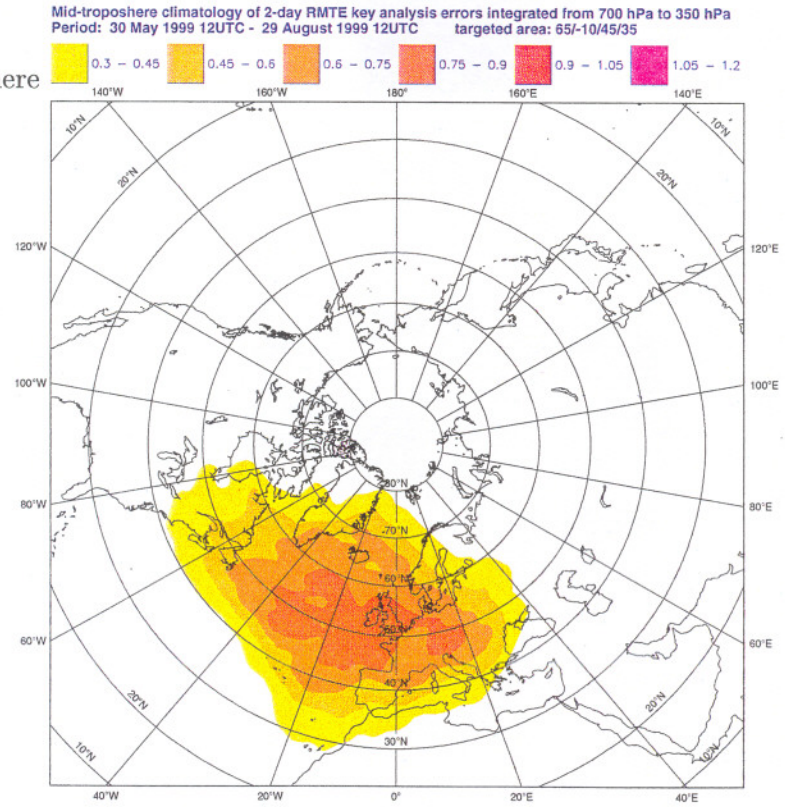

Climatologies Northern Europe, summer

lower troposphere total energy

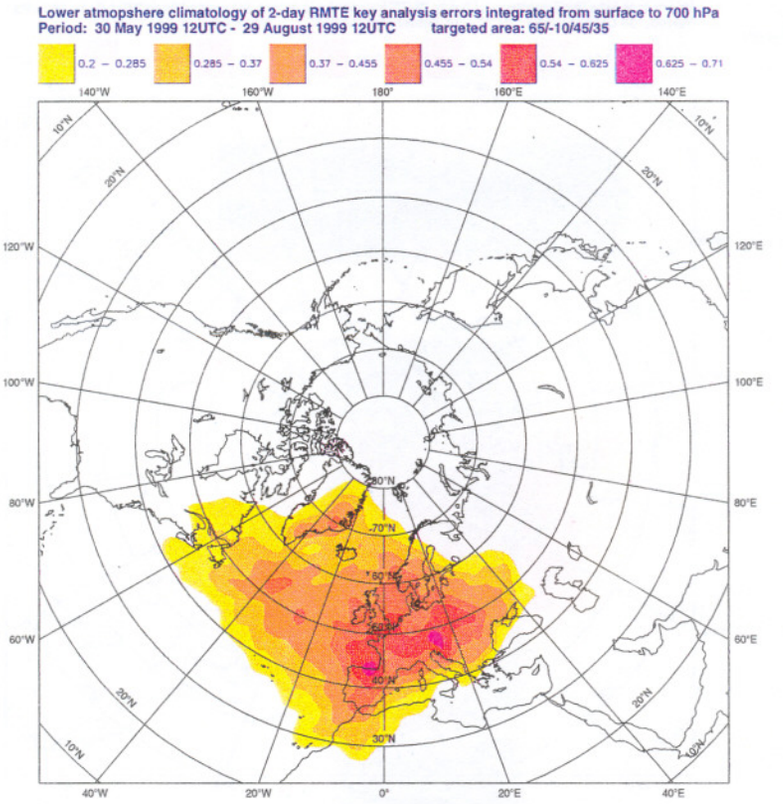

surface pressure

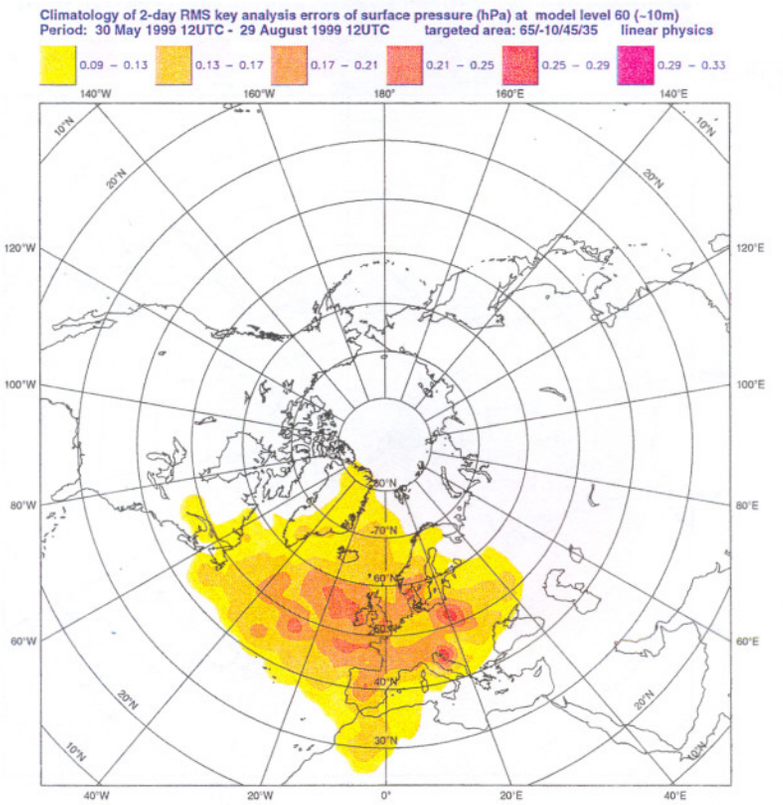

Climatologies Northern Europe, winter

upper troposphere
total energy

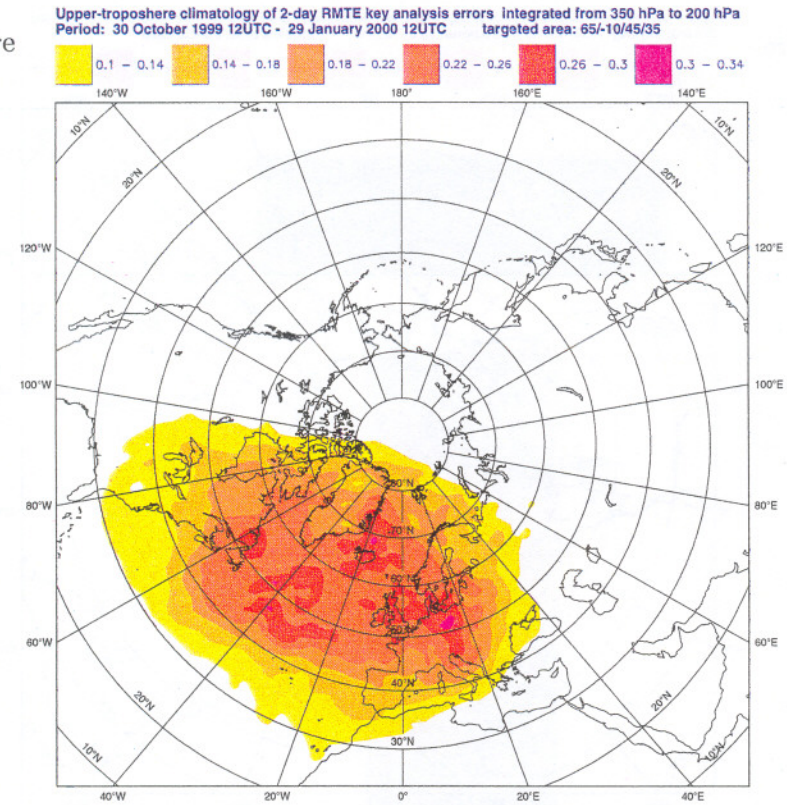

medium troposphere
total energy

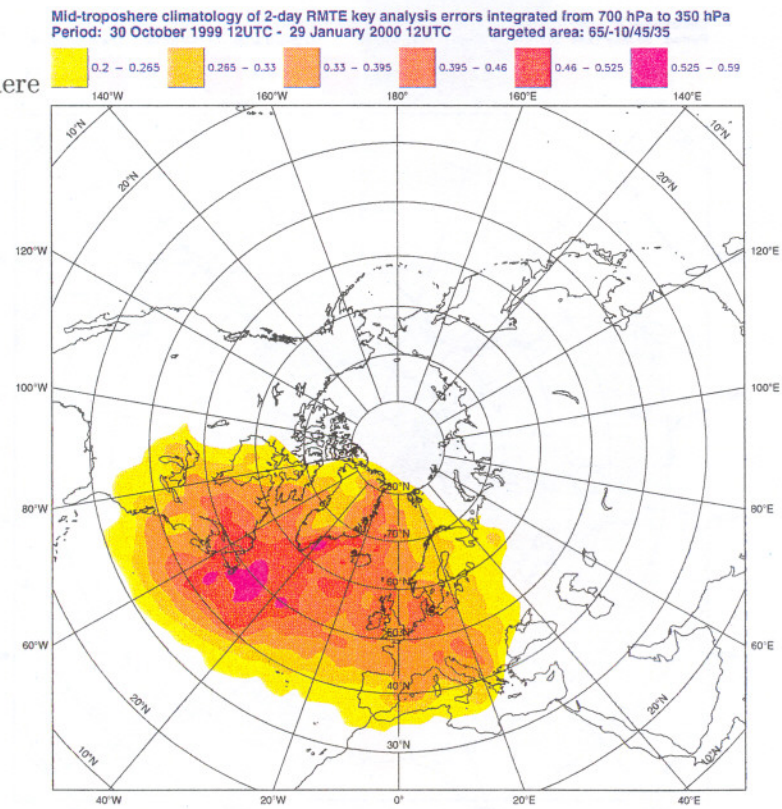

Climatologies Northern Europe, winter

lower troposphere total energy

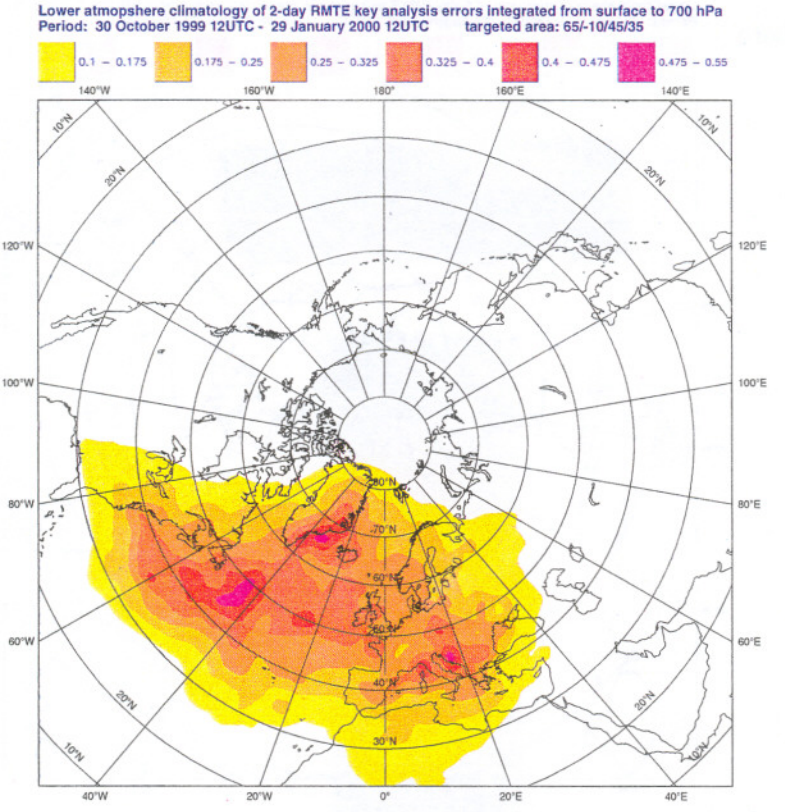

surface pressure

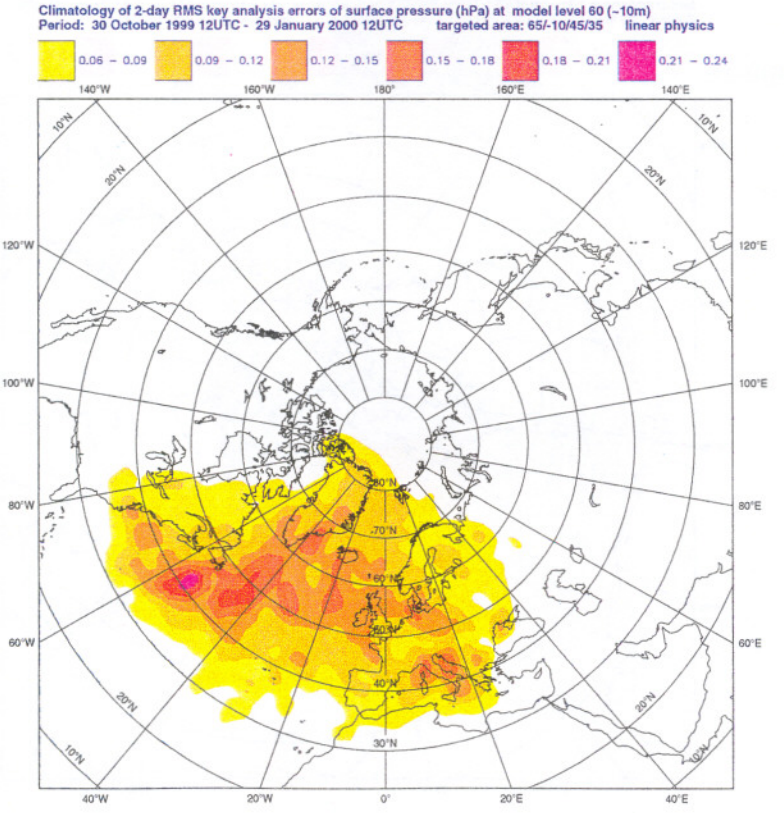

Climatologies Southern Europe, summer

upper troposphere total energy

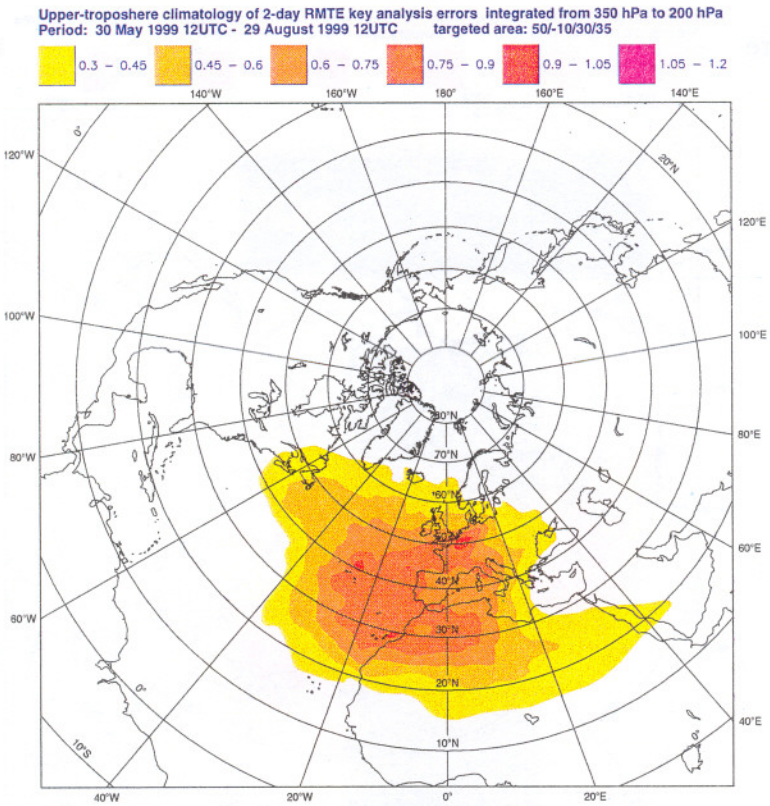

medium troposphere total energy

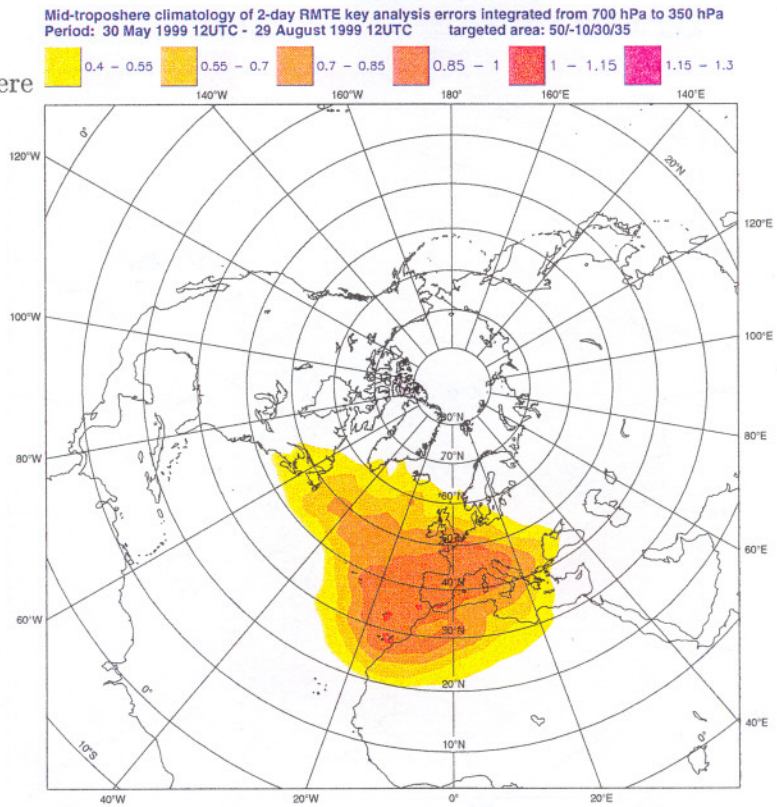

Climatologies Southern Europe, summer

lower troposphere
total energy

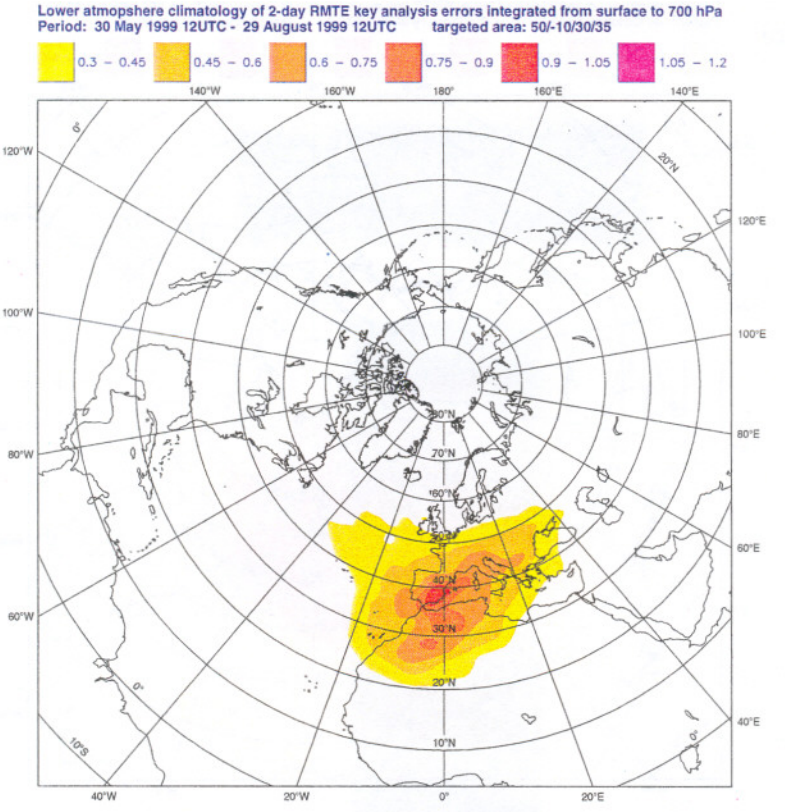

surface
pressure

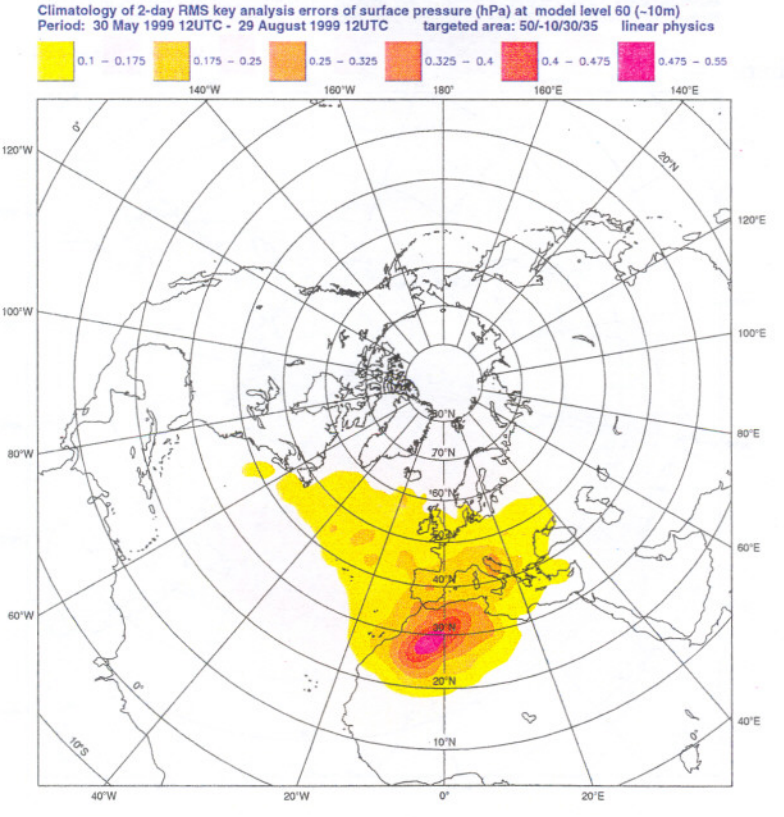

Climatologies Southern Europe, winter

upper troposphere
total energy

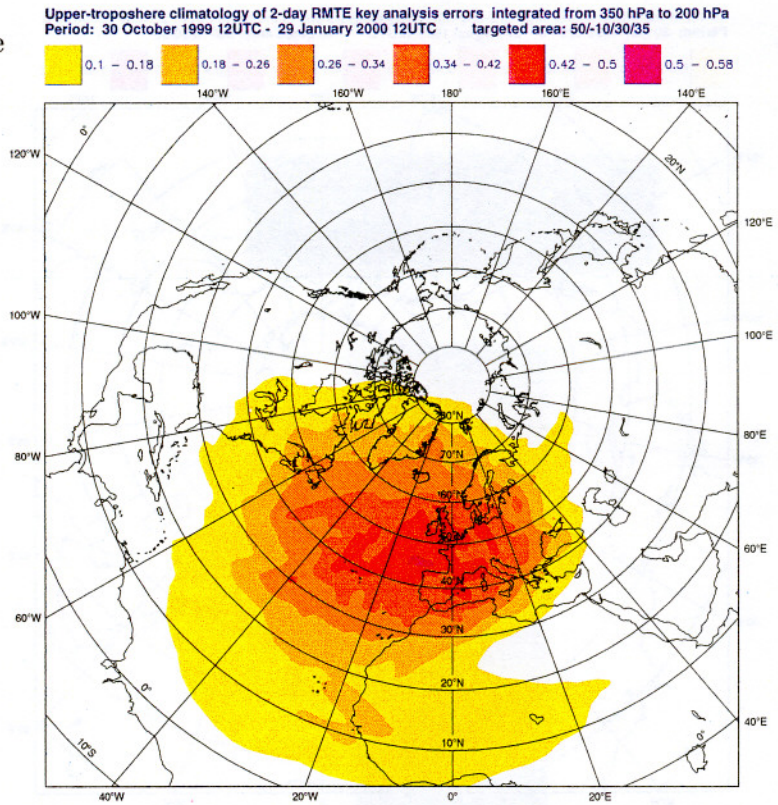

medium troposphere
total energy

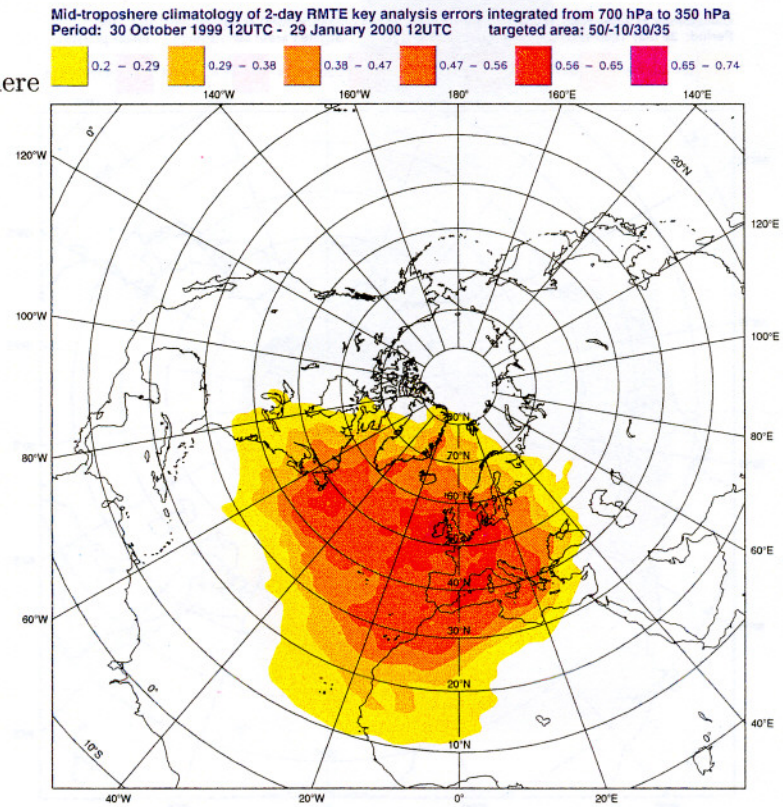

Climatologies Southern Europe, winter

lower troposphere total energy

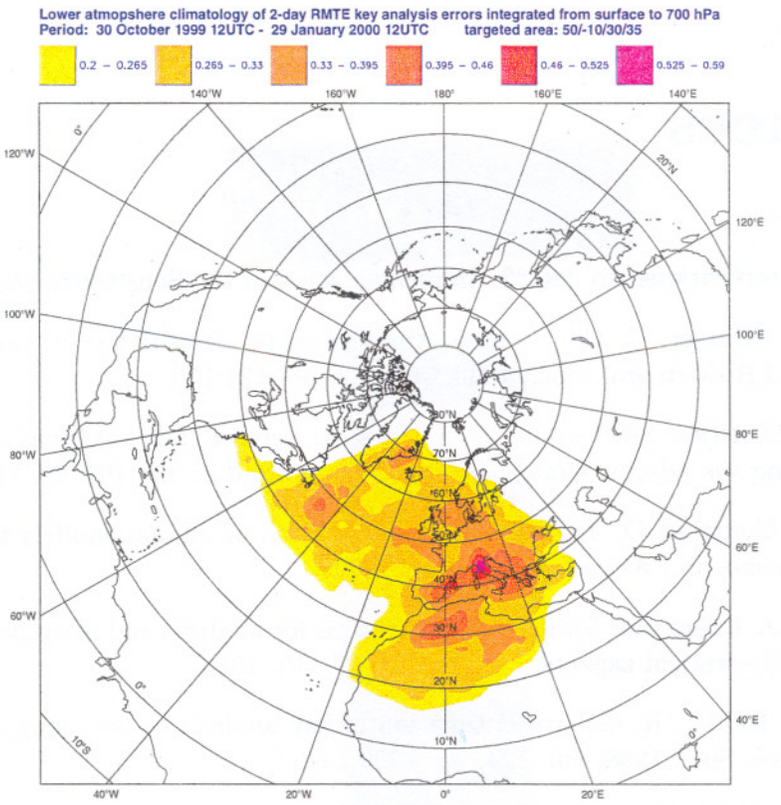

surface pressure

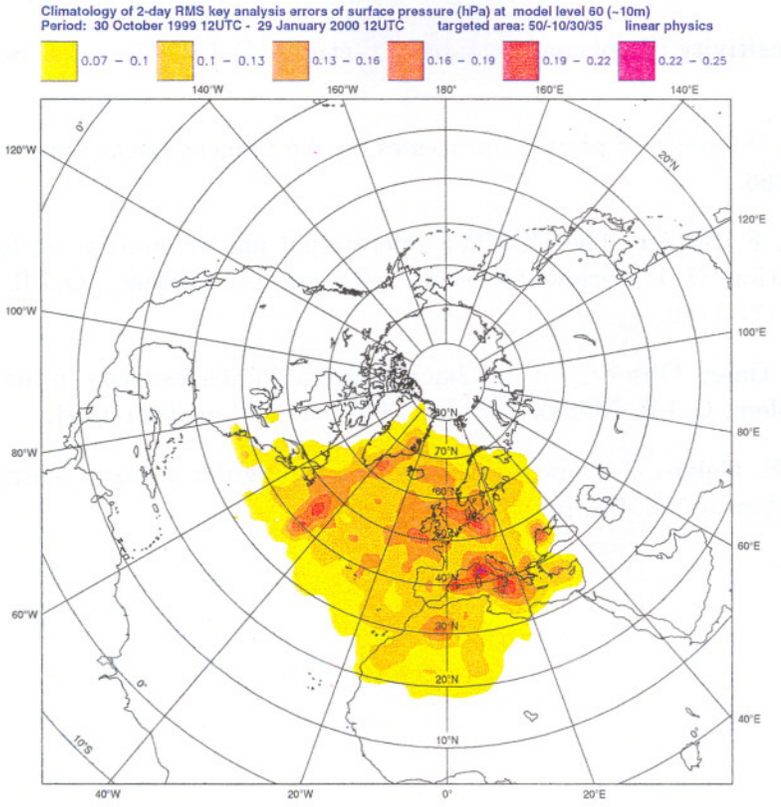

References

[1] F. Gerard, Specifications No. 99/82: Implementation of the Sensitivity Study, January 2000.

[2] F. Rabier, E. Klinker, P. Courtier, A. Hollingsworth, Sensitivity of forecast errors to initial conditions, Q.J.R. Meteorol. Soc., 1996, vol. 122, pp. 121-150.

[3] F. Rabier, P. Courtier, M. Herveou, B. Strauss, A. Persson, Sensitivity of forecast error to initial conditions using the adjoint model, Technical Memorandum no. 197, ECMWF, October 1993.

[4] F. Rabier, P. Courtier, O. Talagrand, An application of adjoint models to sensitivity analysis, Beitr. Phys. Atmosph., August 1992, pp 177-192.

[5] F. Le Dimet, O. Talagrand, Variational algorithms for analysis and assimilation of meteorological observations: theoretical aspects, Tellus, 38A, 97-110. 1986.

[6] E. Klinker, F. Rabier, R. Gelaro, Estimation of key analysis errors using the adjoint technique, Q.J.R. Meteorol. Soc., 1998, vol. 124, pp. 1909-1933.

[7] G.J. Marseille, F. Bouttier, Climatology of Sensitive Areas, EUCOS midterm report, May 2000.

[8] R. Buizza, Sensitivity of optimal unstable structures, Q.J.R. Meteorol. Soc., 1994, vol 120, pp. 429-451.

[9] J.-F. Mahfouf, Influence of physical processes on the tangent-linear approximation, Tellus, 1999, 51A, pp. 147-166.

[10] J.-F. Mahfouf, F. Rabier, The ECMWF operational implementation of four-dimensional variational assimilation. II: Experimental results with improved physics, Q.J.R. Meteorol. Soc., 2000, vol. 126, pp. 1171-1190.

[11] N.L. Baker, R. Daley, Observation and background adjoint sensitivity in the adaptive observation-targeting problem, Q.J.R. Meteorol. Soc., 2000, vol. 126, pp 1431-1454.

[12] T.N. Palmer, R. Gelaro, J. Barkmeijer, R. Buizza, Singular vectors, Metrics, and Adaptive Observations, J. Atmos. Sci. **55**, pp 633-653, feb. 1998